Princeton Plasma Physics Laboratory

PPPL-4257

PPPL-4257

The Discharge Design of HL-2M with the Tokamak Simulation Code (TSC)

Yudong Pan, S.C. Jardin,
and C. Kessel

September 2007

Prepared for the U.S. Department of Energy under Contract DE-AC02-76CH03073.

Princeton Plasma Physics Laboratory
Report Disclaimers

Full Legal Disclaimer

This report was prepared as an account of work sponsored by an agency of the United States Government. Neither the United States Government nor any agency thereof, nor any of their employees, nor any of their contractors, subcontractors or their employees, makes any warranty, express or implied, or assumes any legal liability or responsibility for the accuracy, completeness, or any third party's use or the results of such use of any information, apparatus, product, or process disclosed, or represents that its use would not infringe privately owned rights. Reference herein to any specific commercial product, process, or service by trade name, trademark, manufacturer, or otherwise, does not necessarily constitute or imply its endorsement, recommendation, or favoring by the United States Government or any agency thereof or its contractors or subcontractors. The views and opinions of authors expressed herein do not necessarily state or reflect those of the United States Government or any agency thereof.

Trademark Disclaimer

Reference herein to any specific commercial product, process, or service by trade name, trademark, manufacturer, or otherwise, does not necessarily constitute or imply its endorsement, recommendation, or favoring by the United States Government or any agency thereof or its contractors or subcontractors.

PPPL Report Availability

Princeton Plasma Physics Laboratory:

http://www.pppl.gov/techreports.cfm

Office of Scientific and Technical Information (OSTI):

http://www.osti.gov/bridge

Related Links:

U.S. Department of Energy

Office of Scientific and Technical Information

Fusion Links

The discharge design of HL-2M with the Tokamak Simulation Code (TSC)

Yudong Pan[1], S. C. Jardin[2], C. Kessel[2]

[1]*Southwestern Institute of plasma Physics, SWIP*

[2]*Princeton Plasma Physics Laboratory, Princeton, NJ*

- abstract -

We present results on the discharge design of the HL-2M tokamak, which is to be an upgrade to the existing HL-2A tokamak. We present simulation results for complete 5-sec. discharges, both double null and lower single null, for both ohmic and auxiliary heated discharges. We also discuss the vertical stability properties of the device.

I . Introduction

During the last decade, HL-2A, which originated from the old ASDEX machine, has demonstrated some of the expected benefits of a closed divertor as seen in other tokamaks (Alcator C-mod, ASDEX-U, DIII-D, JET and JT-60U, etc). However, it also has some disadvantages which have limited some more advanced research. These are: an inflexible plasma configuration, weak neutral pumping power in the divertor region, and mechanical trouble from the divertor shaping coils being inside the vacuum vessel, etc, .

HL-2M is to be an upgrade of HL-2A. It will be the largest copper-coil tokamak in China (The other one, EAST, is superconducting). It is designed to operate with elongated plasma cross-sections in either double null (DN) or single null (SN) divertor configurations. The scientific mission of HL-2M is to explore the reactor relevant regimes with high plasma core confinement and to develop and verify solutions for power exhaust and particle control in the presence of high auxiliary heating (10MW in the first step and 20MW in the second step). In the same time, some key technologies and issues related to ITER will be developed. In this report we discuss the design of the poloidal field system and some related issues, such as the estimation of the volt-seconds consumption and poloidal field system stored energy with and without auxiliary heating, and the vertical stability properties.

The Tokamak Simulation Code [1-17] (TSC) is a two-dimensional time dependent free boundary simulation code that advances the MHD equations describing the transport time-scale evolution of an axisymmetric magnetized tokamak plasma. TSC evolves the magnetic field in a rectangular computational domain using the Maxwell MHD equations for the plasma, coupled through boundary conditions to the circuit equations for the tokamak poloidal field coils. The plasma model in TSC is completed by providing functional forms for the electron and ion thermal conductivities, for the particle diffusion coefficients and for the plasma electrical resistivity. We present the results of numerical predictions for the HL-2M discharges which have been carried with the TSC code.

II. HL-2M Poloidal Field coil (PFC) system

Tokamak plasma performance generally improves with increased shaping of the plasma cross section. The newly designed poloidal field coil system must have the capability to accommodate limiter, SN and DN configurations. The cross section of HL-2M PFC system is shown in Fig.1. The major parameters of this design are shown in Table 1. External to the toroidal field (TF) magnet and assembly are the 5 up-down symmetric pairs of primary PF-producing coils. The

central solenoid coil 1, CS1, is divided into two parts by the midplane. PF1 coil has also been divided as two group coils (PF1i, PF1e) but they use same power supply. Because these coils are external to the computational grid, we called them external PF coils. They are labeled in pairs, CS1, CS2, PF1, PF2, PF3 proceeding clockwise around the machine from the high field side to low field side.

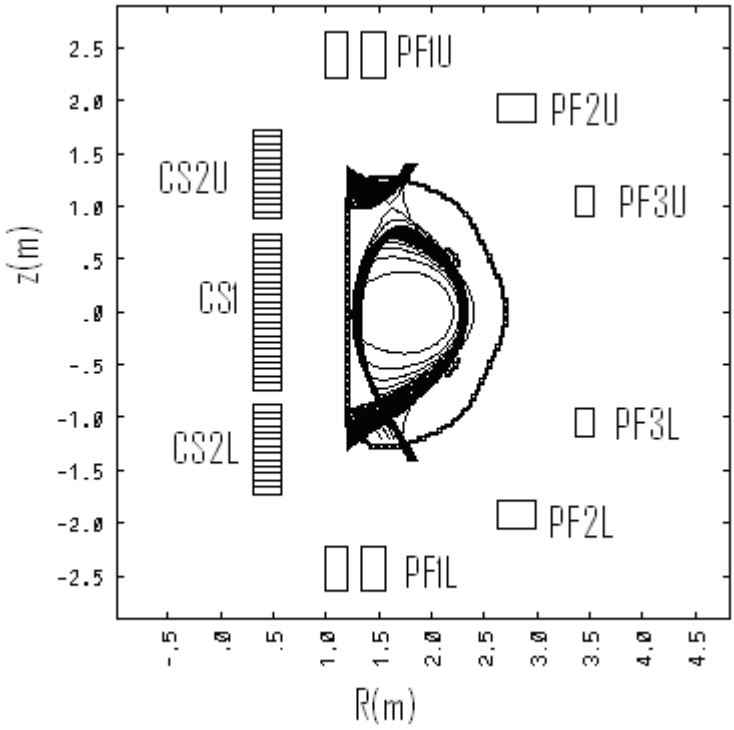

Figure 1: Cross section showing HL-2M poloidal field coil system.

Table1: HL-2M design parameters

Ip(MA)	1.2
Major radius	1.8m
Minor radius	0.5m
R/a	3.6
Elongation at separatrix, κ	1.6~1.8
Triangularity at separatrix, δ	>0.5
Bt	2.6T
$\Delta\Phi(vs)$	10
Flattop time	3s

The first main function of the external coils is to provide the volt-seconds required to build up

and sustain the plasma current by carrying coil currents changing in the opposite direction. The second function is to produce and control the plasma shape. The third function is to provide control of both the radial and vertical plasma position. The detail position and area of each coil are listed in Table 2.

In additional to the external PF coils, there is one pair of passive plates that are being considered to be installed between the plasma edge and vacuum vessel. They are called internal coils. The final design for these is not fixed. An initial evaluation of these is described in Section IV.4. The close-fitting metallic vacuum vessel and the passive plates provide ideal-timescale stabilization to the plasma vertical axisymmetric instability. However, because of the resistivity in these plates, an additional active feedback system is required in order to provide total stabilization.

Table2: Co-ordinates of the poloidal field coils in HL-2M

	Coil radial position R(mm)	Coil poloidal position Z(mm)	Coil height h(mm)	Coil width w(mm)	Coil area/turn h×w mm^2	turns (Nr×Nz)	Maximal available current/turn (kA/turn)	Coil Number	Coil group Number
CS1	440	0	1470	270	55×22	230(10×23)	45	1	1
CS2U(CS2L)	440	1305	840	270	55×22	130(10×13)	45	2,(11)	2,(11)
PF1Ui(PF1Li)	1100	2430	430	220	45×32	54(9×6)	40	3,(10)	3,(10)
PF1Ue(PF1Le)	1450	2430	430	220	45×32	54(9×6)	40	4,(9)	3,(10)
PF2U(PF2L)	2800	1925	270	360	34×47	49(7×7)	37	5,(8)	5,(8)
PF3U(PF3L)	3450	1050	275	185	48×30	25(5×5)	32	6,(7)	6,(7)

III: Typical discharge provided by EFIT code

MHD equilibrium analysis is basic for determining optimal PF coil group current distributions, consistent with engineering constraints. First, the design should include the flexibility of the PF system with respect to different operating modes, for example, double-null divertor (DN), single-null (SN) divertor, limiter, varying elongation and triangularity. Secondly, we must determine the sensitivity of the coil group current distribution to uncertainties in plasma pressure and current distribution and to variations in the plasma shape parameters.

The initial PF coil group currents for each equilibrium conditions (R_0, a, β_{pol}, k) were provided to TSC by using the SWIP version of the equilibrium code EFIT. EFIT is capable of computing equilibrium solutions with fixed plasma profile parameters. Double-null divertor (DN), single-null divertor (SN), and limiter solutions are possible.

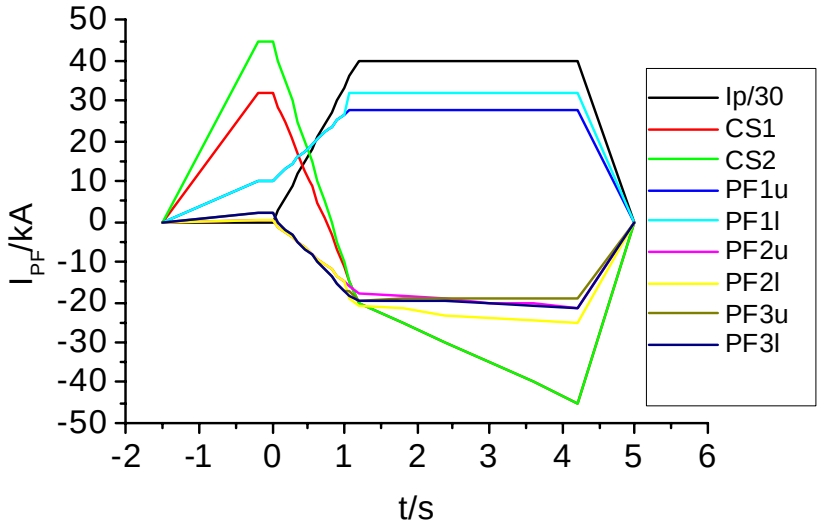

Figure 2: Typical PF coil group currents evolution provided by EFIT code.

Table 3: typical PF coil group current per turn vs. time provided by EFIT code.

T (sec)	Ip (kA)	CS1 (kA/t)	CS2 (kA/t)	PF1U (kA/t)	PF1L (kA/t)	PF2U (kA/t)	PF2L (kA/t)	PF3U (kA/t)	PF3L (kA/t)
-1.5	0	0	0	0	0	0	0	0	0
-0.2	0	32.3	45	10.1	10.1	0.4	0.4	2.2	2.2
0	0	32.3	45	10.1	10.1	0.4	0.4	2.2	2.2
0.09	90	28.36	40	11.63	11.63	-1.4	-1.4	-0.2	-0.2
0.18	180	24.42	35	13.13	13.13	-2.4	-2.4	-2	-2
0.27	270	20.48	30	14.63	14.63	-3.8	-3.8	-3.4	-3.4
0.36	360	16.54	25	16.13	16.13	-5.2	-5.2	-4.8	-4.8
0.45	450	12.6	20	17.63	17.63	-6.4	-6.4	-6.8	-6.8
0.54	540	8.66	15	19.13	19.13	-8	-8	-8.2	-8.2
0.63	630	4.72	10	20.63	20.63	-9.4	-9.4	-9.8	-9.8
0.72	720	0.78	5	22.13	22.13	-10.8	-10.8	-11.6	-11.6
0.81	810	-3.16	0	23.63	23.63	-12	-12	-13.6	-13.6
0.9	900	-7.1	-5	25.13	25.13	-13.4	-13.4	-15.2	-15.2
0.99	990	-11.04	-10	26.63	26.63	-14.6	-14.6	-17.2	-17.2
1.08	1080	-15	-15	28	32	-16.3	-18.9	-17.2	-18.4
1.2	1200	-20	-20	28	32	-17.7	-20.6	-19.4	-19.6

1.8	1200	-25	-25	28	32	-18.3	-21.8	-19.2	-19.4
2.4	1200	-30	-30	28	32	-18.8	-23.2	-19.2	-19.6
3	1200	-35	-35	28	32	-20.1	-24.2	-19	-20.2
3.6	1200	-40	-40	28	32	-20.4	-24.5	-19.2	-20.8
4.2	1200	-45	-45	28	32	-21.4	-25.2	-19.3	-21.2
5	0	0	0	0	0	0	0	0	0

In the next section, we will show the main results from both DN and SN simulations to demonstrate the flexibility of the coil system. The most challenging target is the lower single-null divertor discharge (LSN). Typical LSN preprogrammed waveform of the currents as calculated by EFIT are shown in Fig.2. and Table 3.

IV. Typical discharge provided by TSC code.

The tokamak simulation code is used to simulate the current ramp up, flattop and ramp-down phases of normal HL-2M discharges. TSC includes a two-dimensional transport description of the plasma, using neoclassical resistivity. In these simulations we used the Coppi-Tang two-regime anomalous thermal conductivity model [2] with $\chi_i = \chi_e$. The temperature profiles Te,i(ψ, t) are evolved self-consistently. However, the density profile is fixed in shape for all time while the central density is given prescribed time dependence. In these simulations, we used a time-averaged sawtooth model in which no attempt is made to simulate the detailed dynamics of sawtooth. Instead, the effect of sawteeth on the temperature and current density evolution is taken into account, in the average sense, by flattening the resistivity profile inside the sawtooth inversion radius according to the prescription

$$\eta_{//} = \eta_{NC}, \quad \text{For} \quad q \geq 1 \tag{1}$$

$$\eta_{//} = 0.5\eta_{NC} + 0.5\eta_{NC}|_{q=1}, \quad \text{For} \quad q < 1.$$

The first task for our TSC simulation is benchmarking the results from EFIT. The simulations presented here are (a) a DN (Double-null divertor) discharge with Ip = 1.2MA (DN). (b) The same current level discharge in LSN (lower single null divertor)

The whole computational domain is covers a width from 1.05m to 2.85m in the R direction and a height from -1.4m to 1.4m in the Z direction. This is resolved using 116 vertical divisions (zones) and 73 radial divisions as shown in Fig. 3.

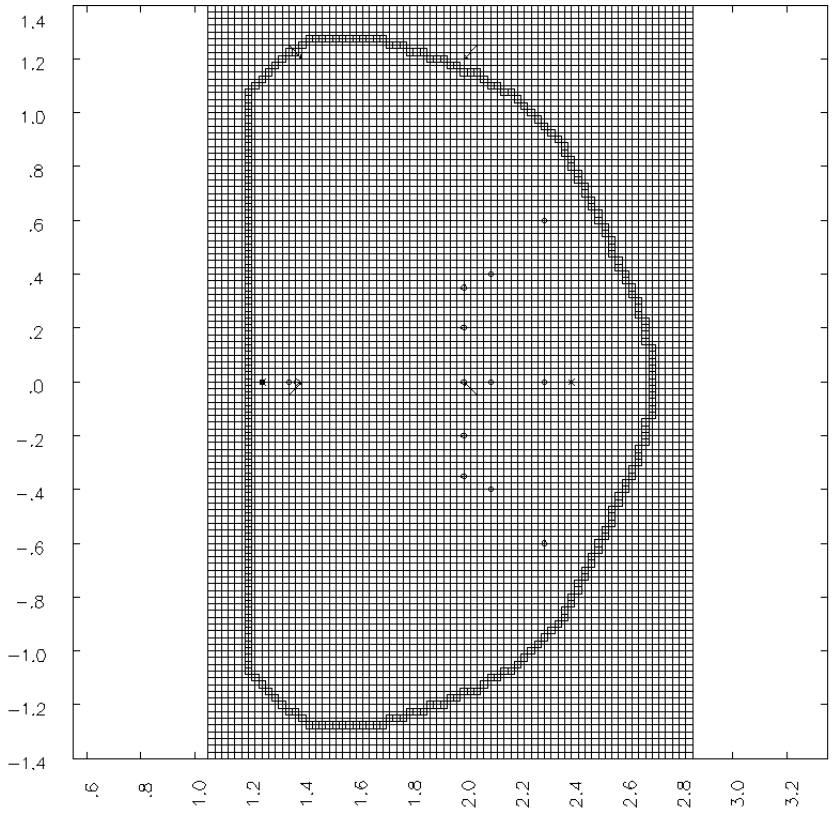

Figure 3: TSC computational domain for the HL-2M tokamak.

IV.1 Ohmic heating DN divertor discharge

The basic HL-2M design should have DN divertor discharge capability. The nominal currents in each PF coil are listed in Table 3. However, if symmetric magnetic surfaces (for a DN discharge) are desired, only the current values listed for the upper coils are used for both the upper and the lower coils. In the ohmic discharge, most of the important plasma profile parameters and flux linkage at the BOFT (beginning of flattop), Flattop, EOB (end of flattop) are given in Table 4. The main parameters of the evolution are presented in Fig.4~Fig.20.

The plasma current is ramped linearly in time from the initial value Ip=50 kA at time=0.0s to the flattop value of Ip=1.2 MA at t=0.99 sec (Fig5), then remains constant until 4.2sec and ramps down linearly to 0.0 kA at 5sec. The toroidal field change is not plotted as it is kept at Bt=2.5 T. The plasma electron density (Fig.8) linearly increases to it's highest value, $n_0 = 8\times10^{19}\,m^{-3}$ at 1.2sec, then stays constant until 4.2 sec, and drops down to zero linearly at the end of discharge.

Through arranging the observing flux-loop pair positions appropriately and with reasonable radial feedback gain factors, TSC can stabilize the plasma magnetic axis position (XMAG=1.85m,

ZMAG=0m) from 0.5sec. (Fig5, Fig6). Fig.6 also indicates that two X-points are formed (indicated by IPLIM = -2) from 0.5 sec and retained throughout the discharge. The plasma major radius retains the value of 1.83m from 0.5sec and keeps this to the end of the flattop while the plasma minor radius shrinks from 0.56m to 0.53m during the flattop phase (Fig.11). Fig4 shows superimposed snapshots of the plasma/vacuum interface at various times during the plasma evolution. The plasma is grown from an inboard limited circular plasma at t=0.0sec, became diverted from 0.5sec, and achieve a stable elongation of k_{95}=1.6 at the beginning of the flattop. Plasma triangularity and elongation all (Fig.12) keep quite stable during the flattop. Fig13 shows the evolution of the X-points. Fig.19 and Fig. 20 show the plasma profile parameters: The central beta β is about 1.0 %, the sum of plasma internal inductance $l_i/2$ and plasma poloidal beta β_p is about 1.0. Plasma internal energy in most of the flattop phase stays constant 0.28MJ (Fig8) while the plasma energy confinement time keeps going down from 180 to 150ms (Fig9.). The plasma central electron temperature Te (Fig10) approaches 1.5 keV in the flattop.

Fig7 shows the calculated edge safety factor as a function of time. Several definitions of q_{edge} are possible. In the flattop phase, q_0 is lower than 1 and q_{edge}(95%) is about 3.5~4. A higher edge q factor provides assurance against disruptions.

Fig14 shows a plot of volt-second consumption. A total 10.5 Volt-seconds are required by the PF system to reach EOFT, of which 6.5Volt-seconds are due to resistive losses. Fig16 shows the actual total current in each PFC group. Fig.17 shows the detail Volts-s contribution from each coil group. It is seen that the CS1 and CS2 coil groups are main Volts-sec provider. PF3 (Coil group 6 and 7) has no contribution to the total V-s but it is necessary to maintain the plasma shape. At about 3.0sec, Fig16 shows that the Volts-sec are used up because the currents in CS1 and CS2 coil arrive their total available maximal currents 5175kA and 5850kA. Fig. 15 is the total plasma ohmic power balance and Fig.18 is the total power requirement to the PFC system.

Table 4.Fixed plasma parameter for DN discharges

	BOFT	Flattop	EOB
Time(sec)	1.0	3.0	4.2
Plasma current(MA)	1.01	1.2	1.12
Major radius(m)	1.815	1.818	1.818
Minor radius(m)	0.55	0.535	0.522
Elongation (95%)	1.57	1.579	1.554
Triangularity (95%)	0.224	0.256	0.259

Flux linkage(V-s)	5.2	9.0	10.5
Field on axis(T)	2.5	2.5	2.5
beta β (based on actual toroidal field)	0.00254	0.00396	0.00386
Poloidal beta β_p	0.294	0.30	0.315
Internal inductance $l_i/2$	0.582	0.556	0.584

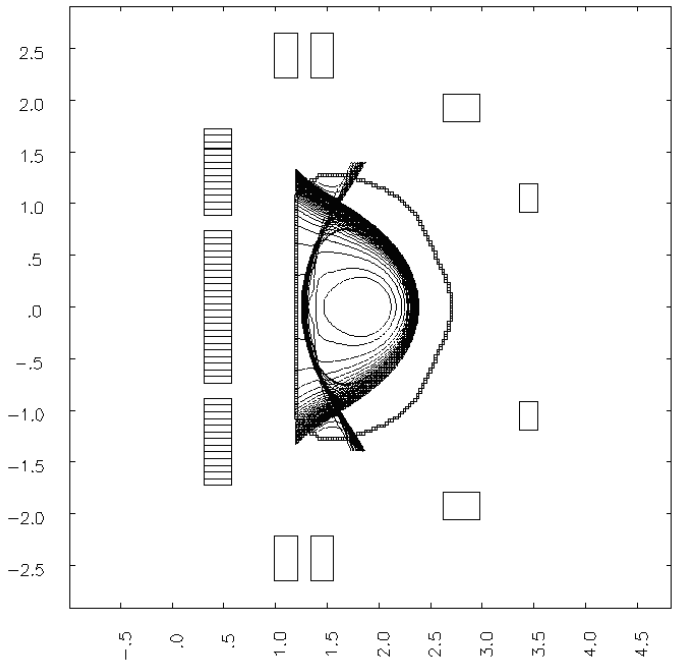

Fig 4: Snapshots of the DN plasma/vacuum interface at various times during the evolution from 1 sec to 5sec.

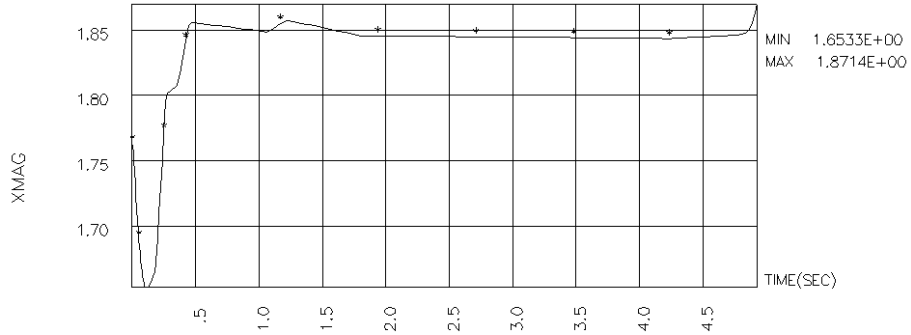

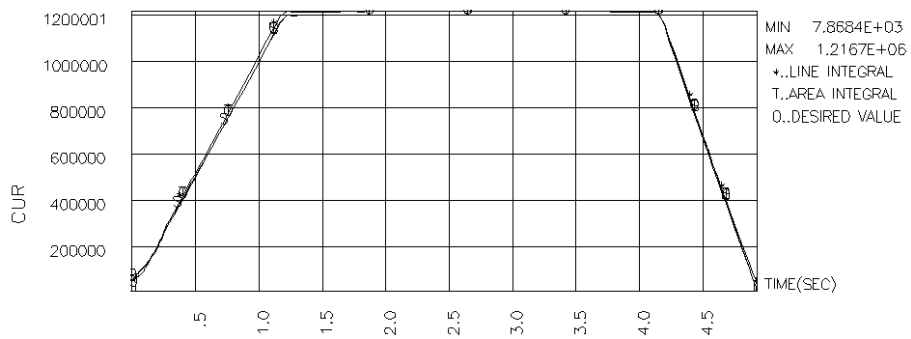

Fig5: Evolution of plasma current CUR and plasma magnetic axis horizontal displacement XMAG in ohmic heating DN discharge. Bottom graph contains three curves indicating pre-programmed(0), and two measures of the actual(T,*) plasma current.

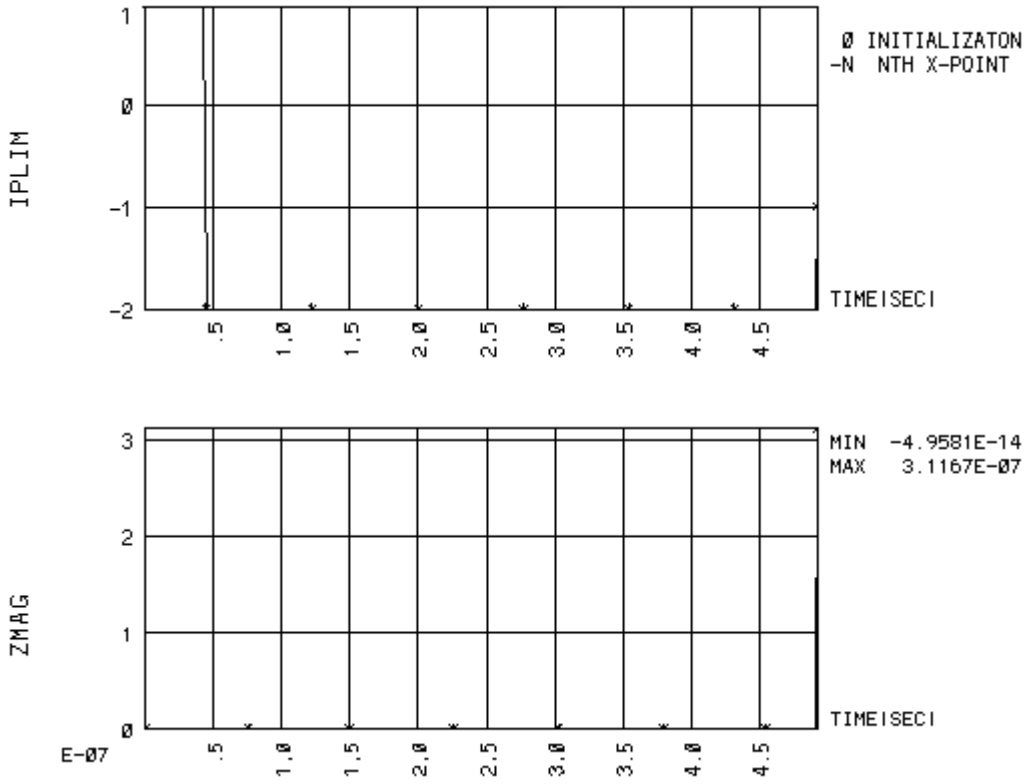

Fig6: (Top) DN discharge first has limiter configuration until 0.5sec, then changes to two X-point (IPLIM=-2). (Bottom) Evolution of plasma magnetic axis vertical displacement ZMAG in ohmic heating DN discharge.

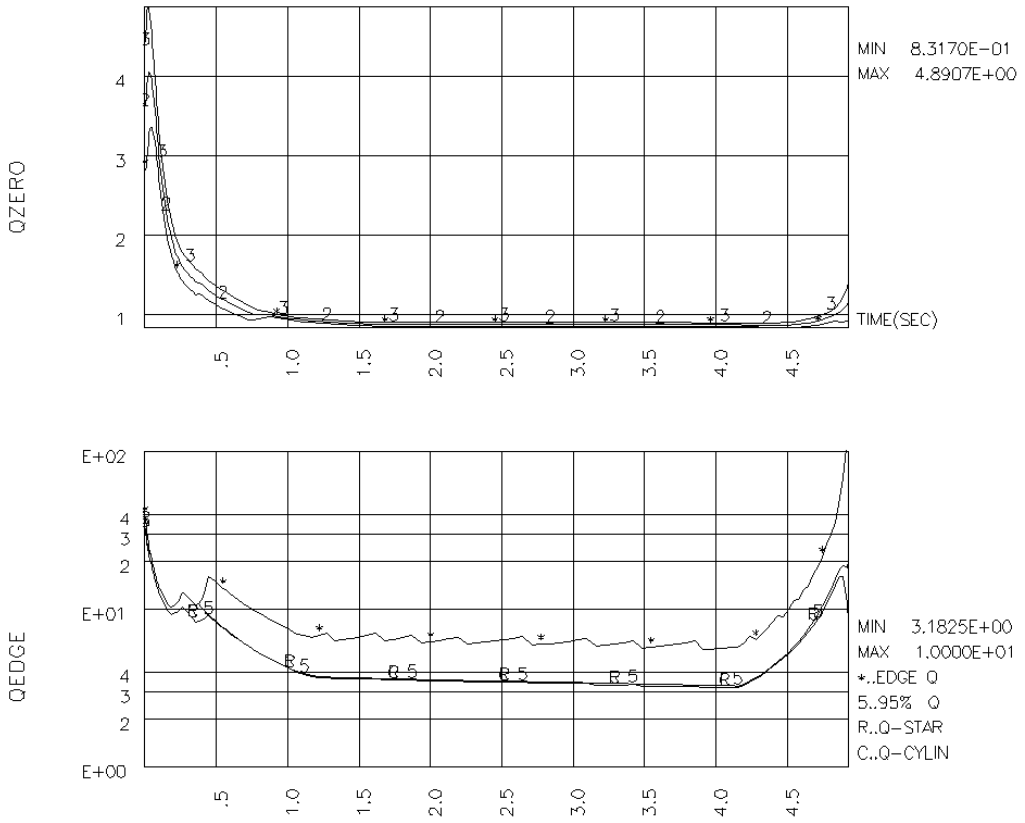

Figure 7: Evolution of plasma q factors in the plasma edge (bottom) and plasma central (top).

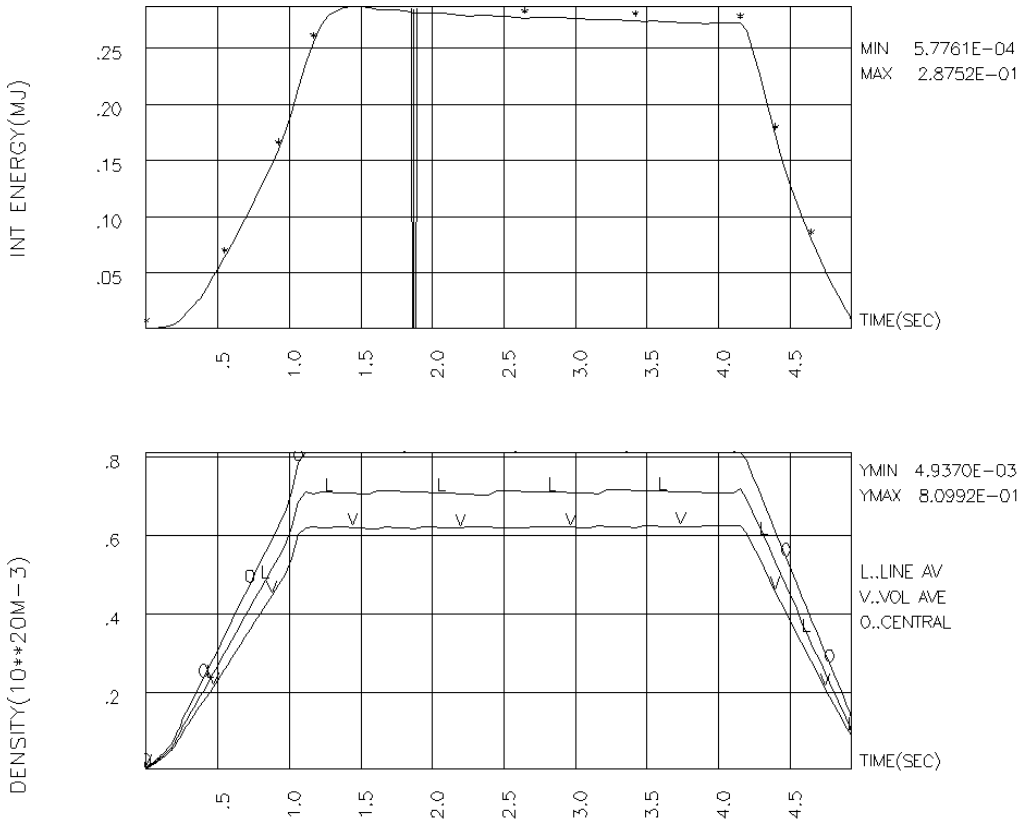

Figure 8: Evolution of plasma internal energy (top) and plasma electron density (bottom) in ohmic heating DN discharge.

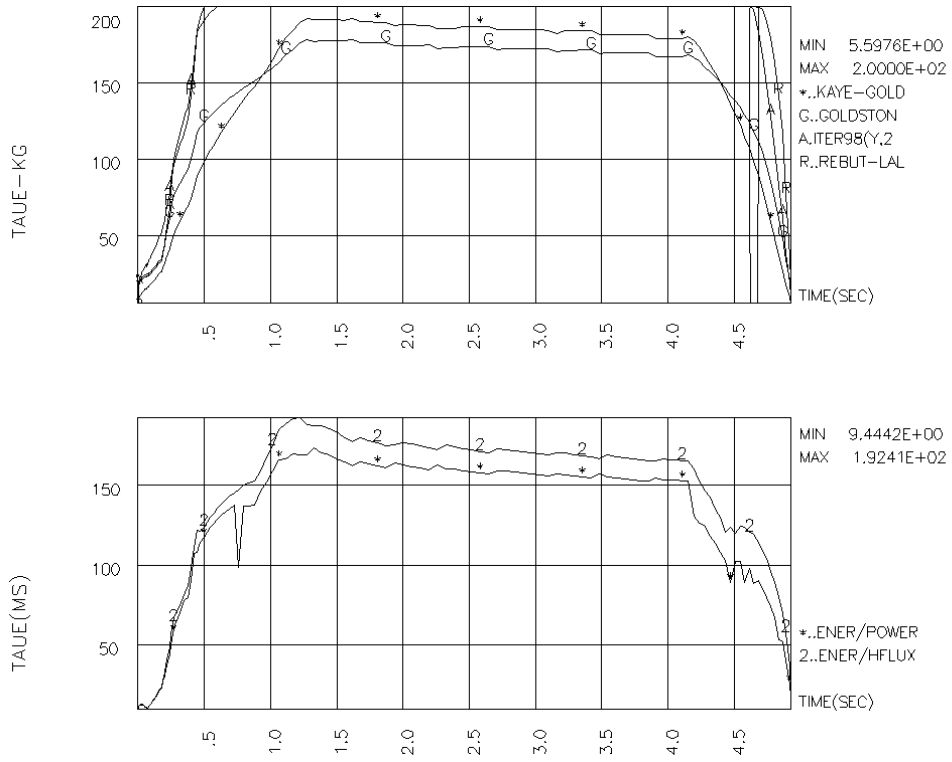

Figure 9: Evolution of plasma energy confinement time calculated in different scaling law.

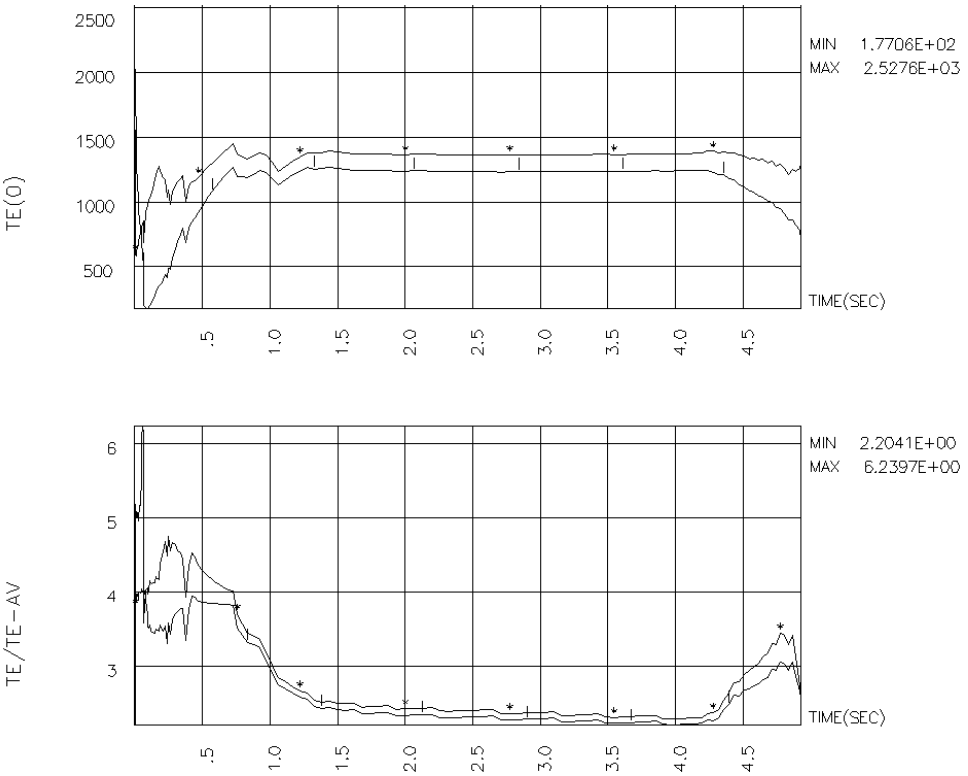

Figure. 10: Evolution of central electron and ion temperature Te,i(0) and peak to average temperatures Te,i(0)/<Te,i> for ohmical DN discharge simulation.

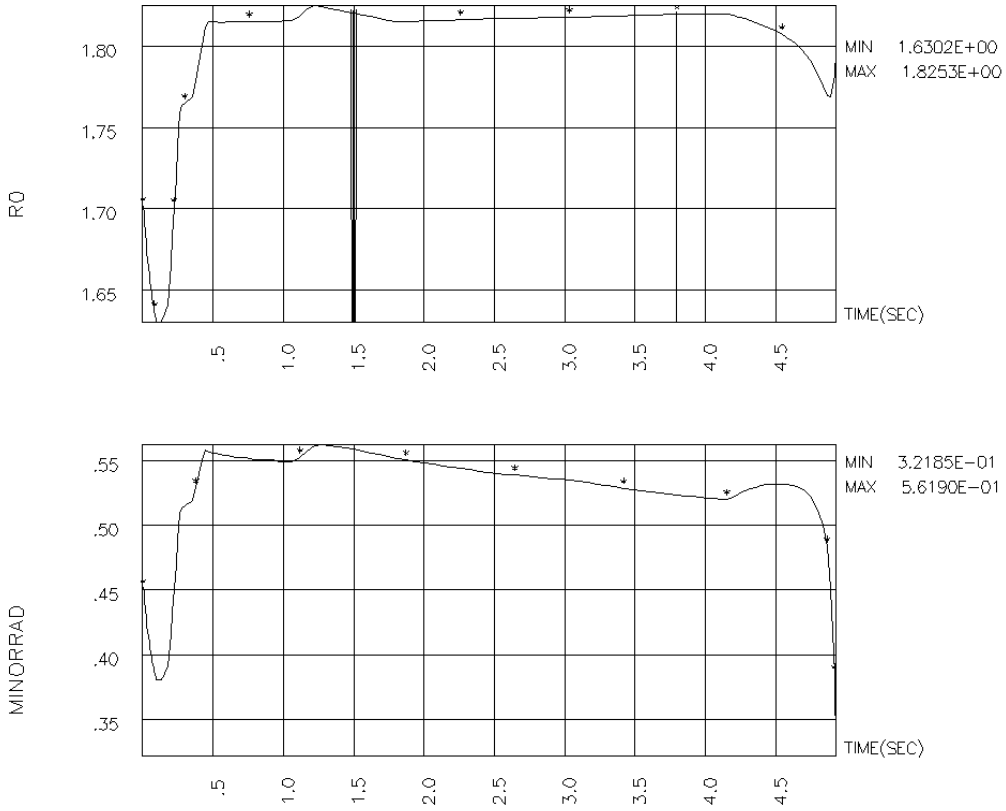

Figure.11: Evolution of major radius R_0 and minor radius r for ohmic heating DN discharge.

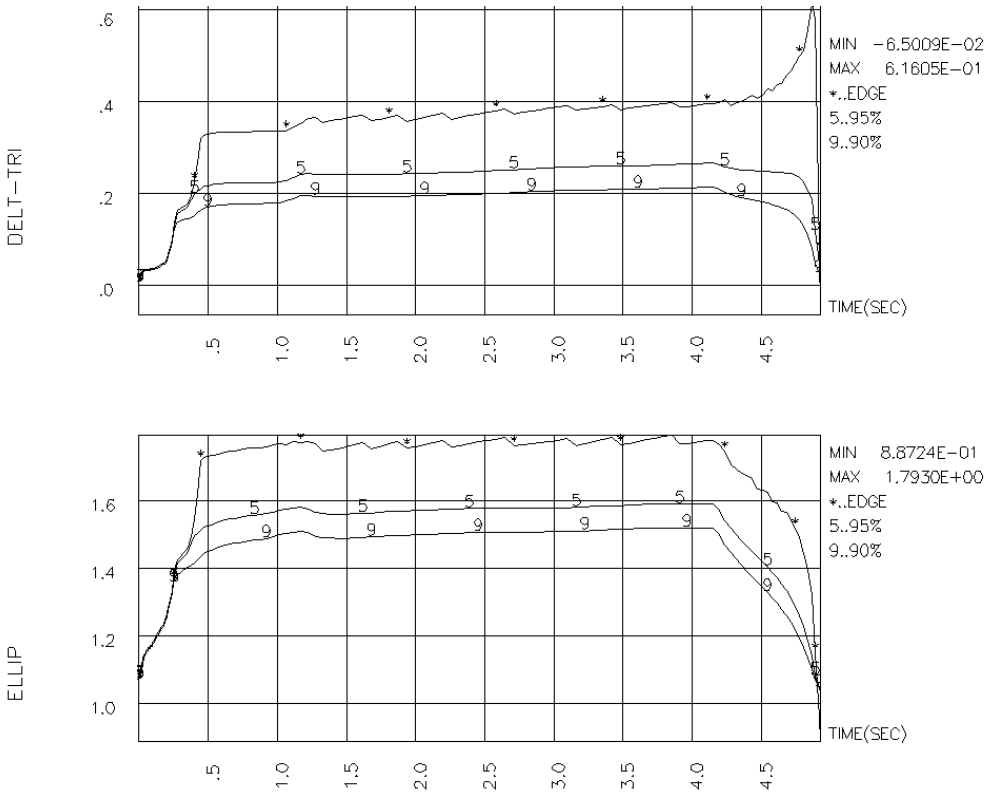

Figure 12: Evolution of triangularity (top) and elongation (bottom) for DN ohmic discharge. The symbol 5 indicates the 95% flux surface,9 indicates the 90% flux surface and * indicates the plasma boundary.

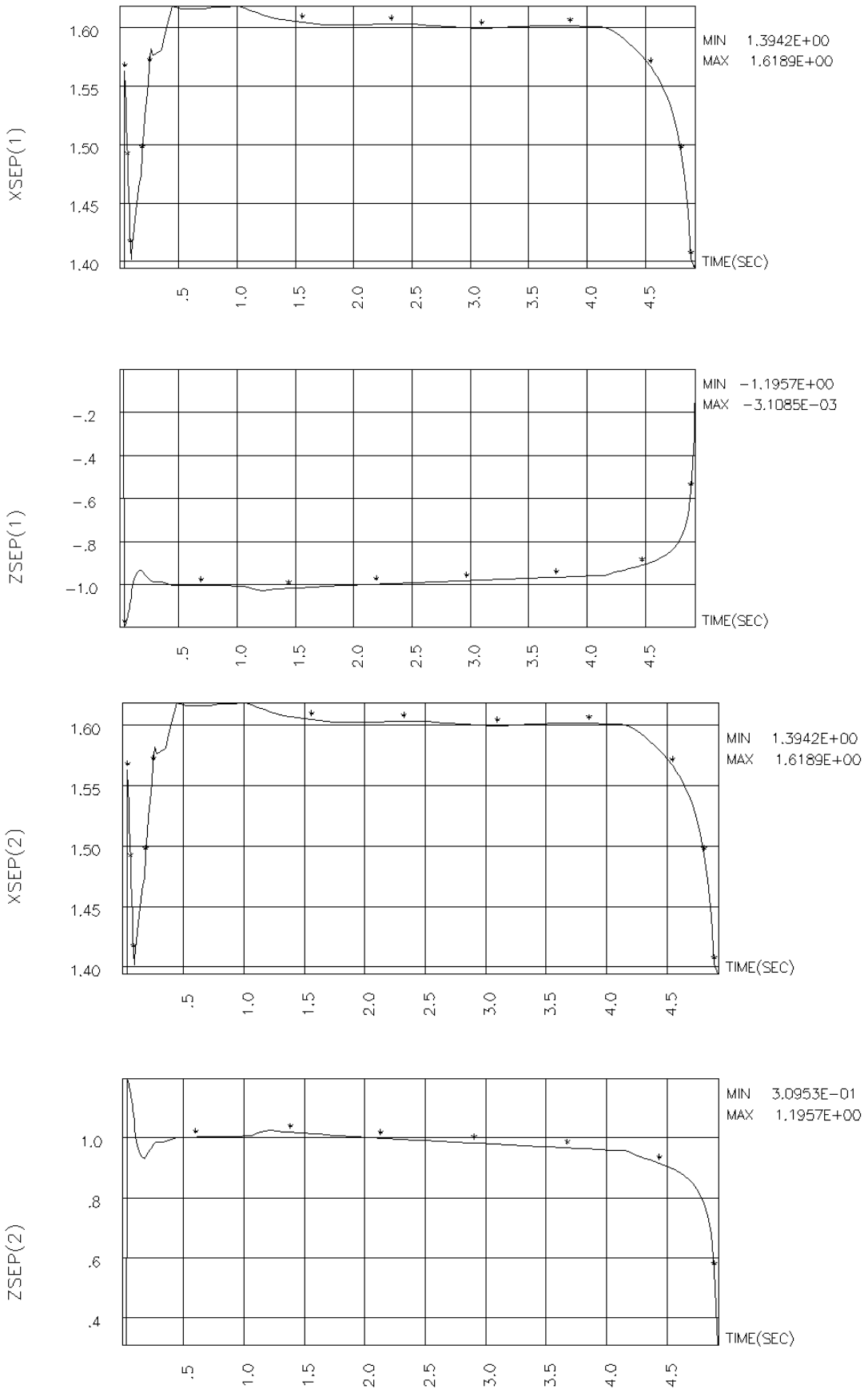

Figure 13: Evolution of two active X-Points in DN ohmic discharge.

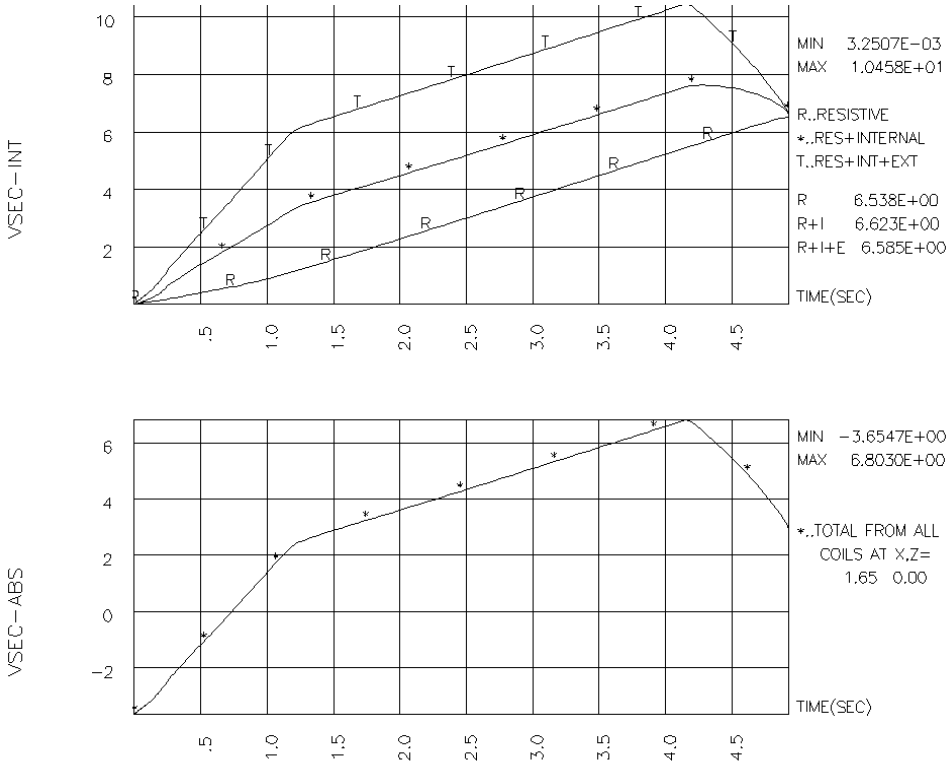

Figure14: Evolution of Volt-seconds (top) and its absolute value.

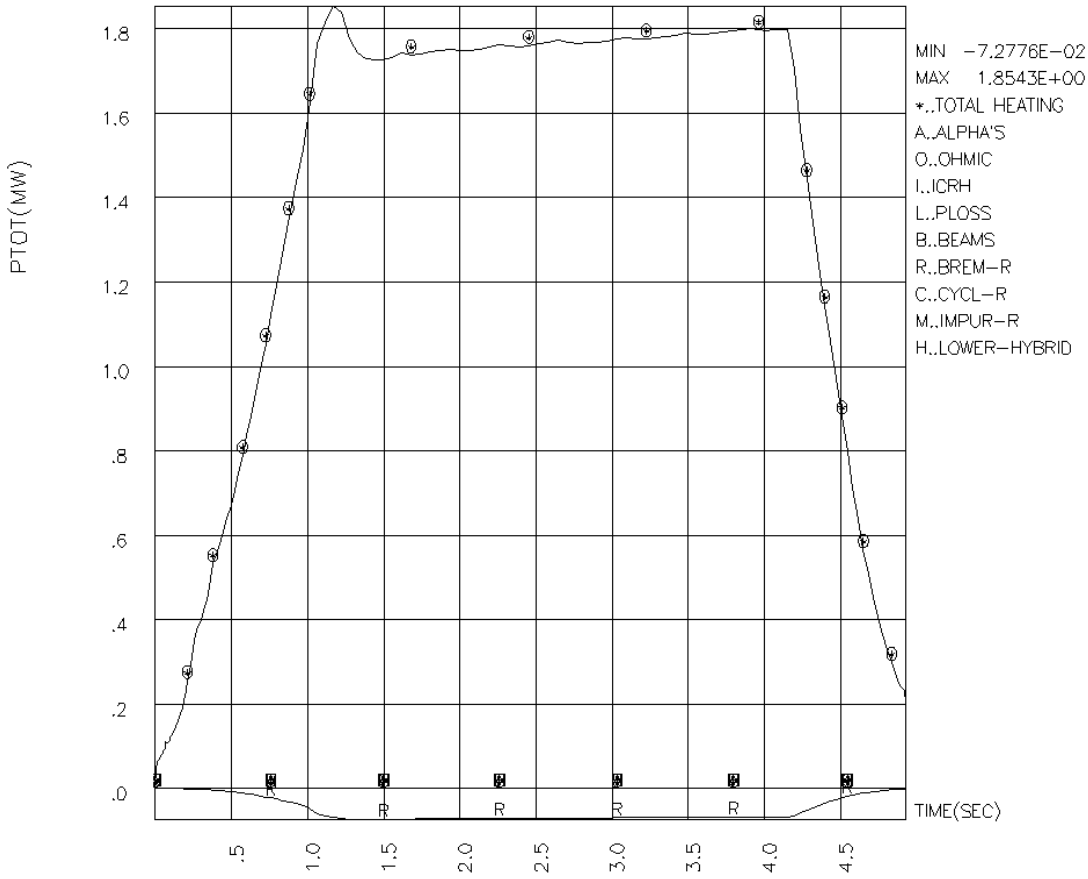

Figure 15: Plasma power balance vs. time for an ohmical DN discharge.

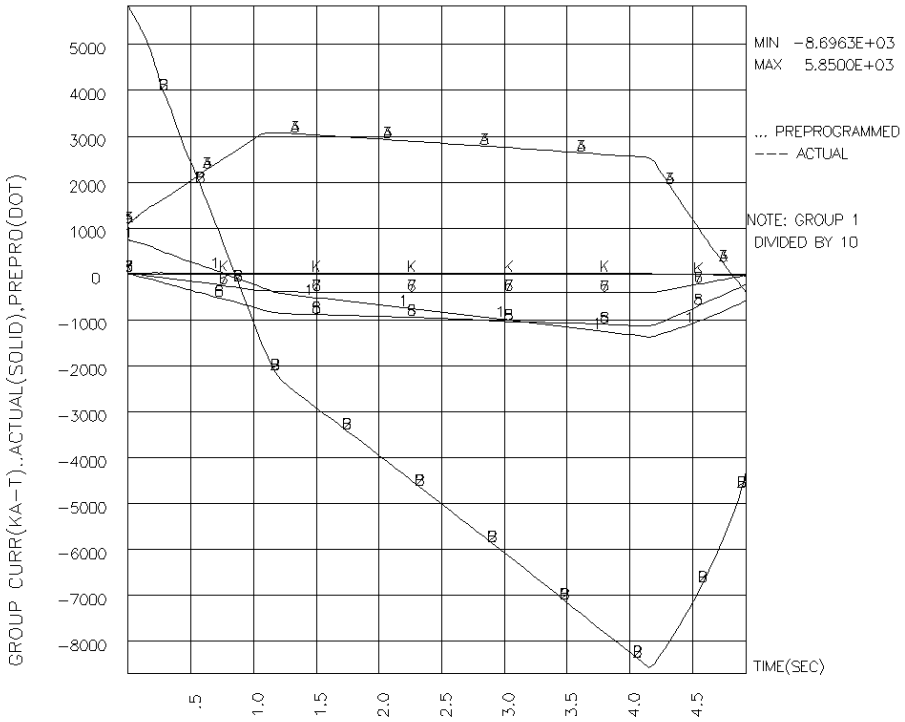

Figure 16: The histories of PF coil group currents (upper+lower half plane values) for the ohmic heating DN discharge.

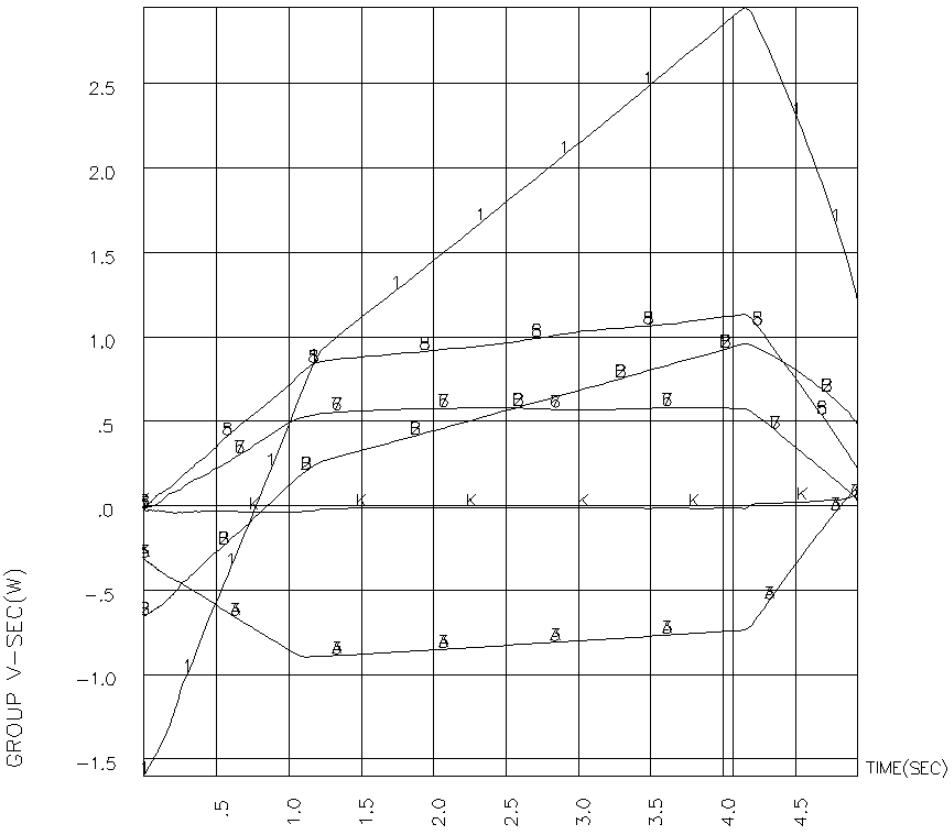

Figure 17: Volt-sec contribution from PFC.

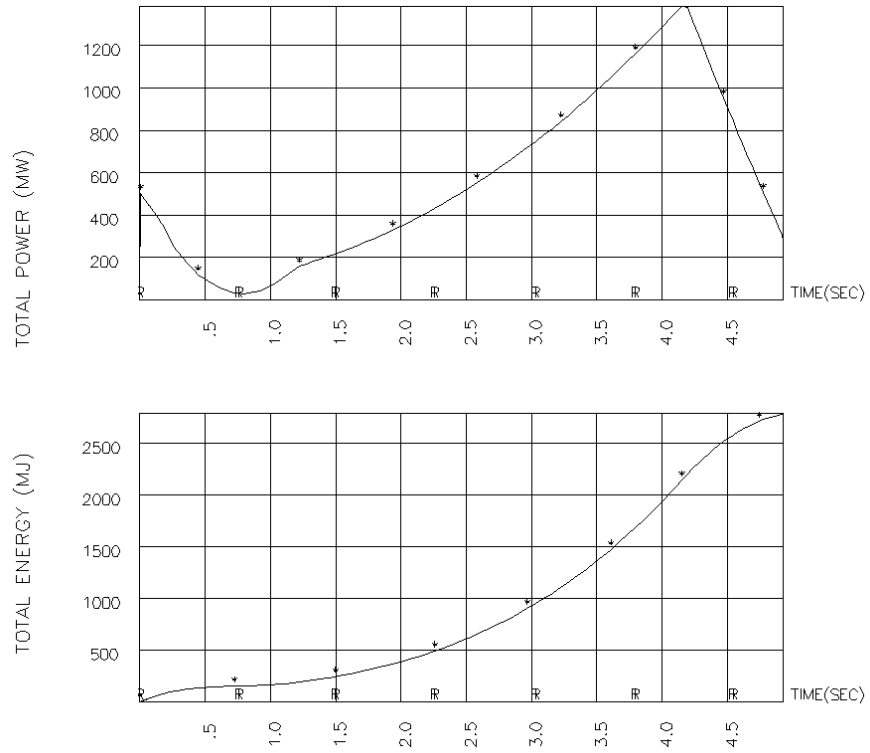

Figure 18: Evolution of total energy and total power in poloidal field coil system.

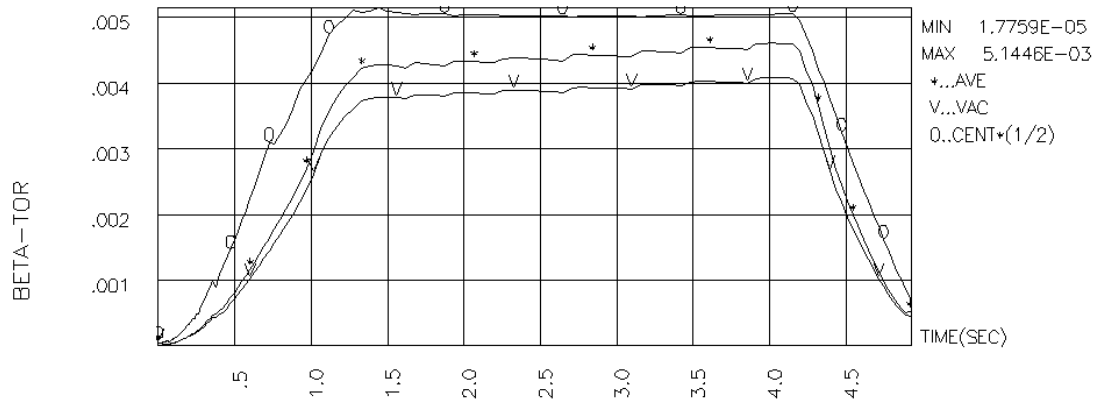

Figure.19. Evolution of one-half central beta (0), beta based on vacuum field (v), and beta based on actual toroidal field (*).

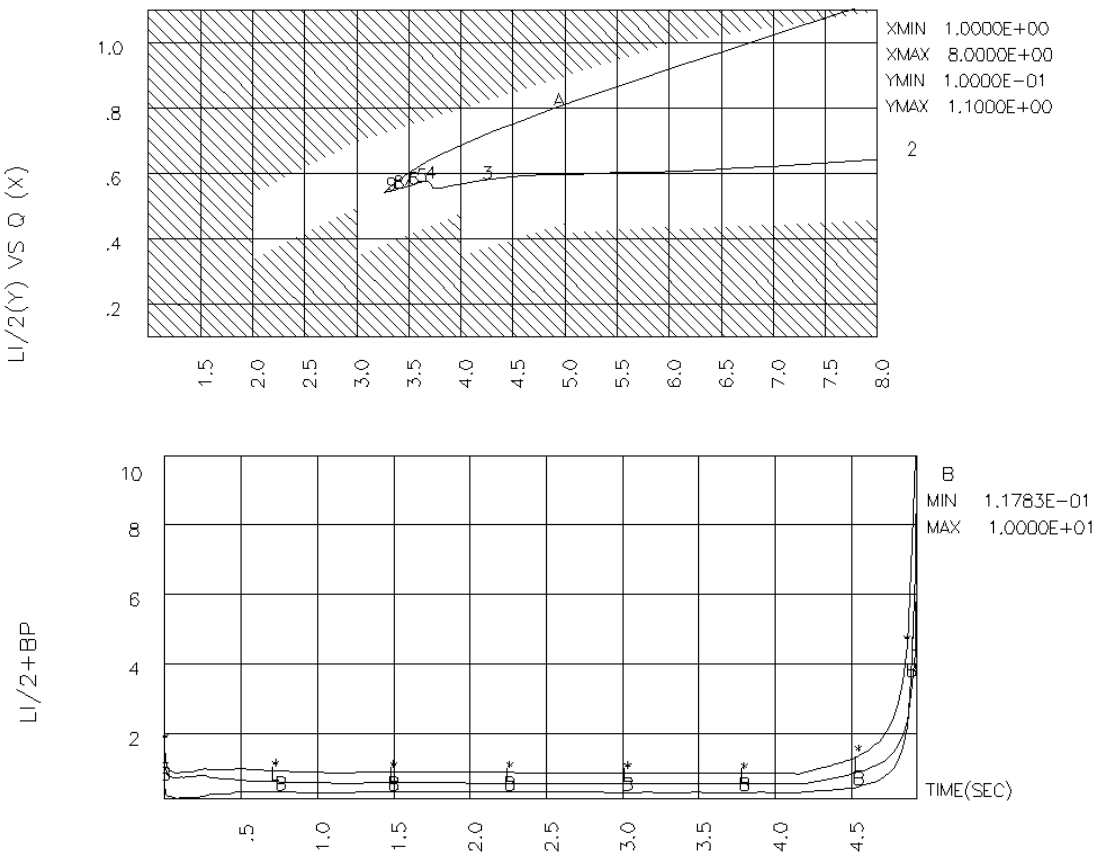

Figure 20. Bottom: Evolution of internal inductance $l_i/2$, poloidal beta β_p , and the sum $l_i/2+\beta_p$. Top: the evolution of plasma in space of internal inductance $l_i/2$ versus edge safety factor q_{95}. Unshaded region is stable according to model calculation.

IV.2 LSN discharge

The standard HL-2M plasma is a lower single null divertor discharge in order to maximize the plasma volume within the vacuum vessel. In this case, the position of the active X-point (assumed here is the lower null), flux Volt-second consumption, and the plasma shape are the focus.

Single-null plasma parameters for BOFT, Flattop, and EOB are listed in Table 5 and many features of the plasma evolution is displayed in Table 5 and Figures.21 to 40.

Most of the main plasma parameters are set the same as that in DN case, such as plasma current waveform (Fig. 22), plasma electron density waveform (Fig.25), observing pair positions, etc. The difference between these two configurations is that we force a stronger pre-programmed current to pass through most of the coil groups in the lower midplane region to form the lower SN configuration.

The designed discharge begins as a limiter configuration for the first 0.5sec, then changes to double null divertor until 1 second. Due to the asymmetric current beginning at 1 second, Fig.23

shows one active X-point formed immediately from 1 second and retained all discharge (IPLIM = -1). Fig 22 shows that the plasma magnetic axis radial position is around XMAG=1.83m. The vertical displacement of the magnetic axis shifts down from the beginning of flattop, the maximal displacement is about ZMAG=0.07m at the end of flattop (Fig.23).

Compared with the fixed plasma radius in DN configuration, the plasma major radius in LSN configuration is reduced to 1.80m (a little less) from 0.5sec and keeps this value to the end of flattop. The plasma minor radius shrinks from 0.55m to 0.49m during the flattop phase (Fig.28). Plasma triangularity and elongation (Fig.29) are stable but are also lower than that in the DN. Fig.30 shows X-positions evolution in LSN configuration. The active X-point is about 1.0m lower than the midplane. Fig.35 and Fig. 36 show the plasma profile parameters, that the central beta β still equal to 1.0 %, the sum of plasma internal inductance $l_i/2$ and plasma poloidal beta β_p is still about 1.0. The beta based on vacuum field (listed in table 5) is a little different to that at DN configuration due to a slight difference in plasma shape.

The safety factor q at plasma center and edge shown in Fig 24 are comparable to those in the DN. The plasma internal energy (Fig.25), plasma energy confinement time (Fig26.), and central electron temperature Te (Fig20) also are very similar to those in the DN.

Fig31 is the total discharge Volts-sec consumption. Fig33 shows the actual total current in each of the PF coil groups. Also at about 3.0sec, the Volts-sec is used up. Fig. 32 is the total plasma power balance. Fig.34 is the total power consumption by the PF coil groups

Table 5.Fixed plasma parameter for LSN discharges

	BOFT	Flattop	EOB
Time(sec)	1.0	3.0	4.0
Plasma current(MA)	1.02	1.2	1.2
Major radius(m)	1.80	1.80	1.80
Minor radius(m)	0.54	0.50	0.50
Elongation (95%)	1.575	1.533	1.535
Triangularity (95%)	0.218	0.22	0.22
Flux linkage(V-s)	5.56	8.2	9.0
Field on axis(T)	2.5	2.5	2.5
beta β (based on actual toroidal field)	0.0025	0.0045	0.00442

Poloidal beta β_p	0.293	0.27	0.26
Internal inductance $l_i/2$	0.583	0.530	0.516

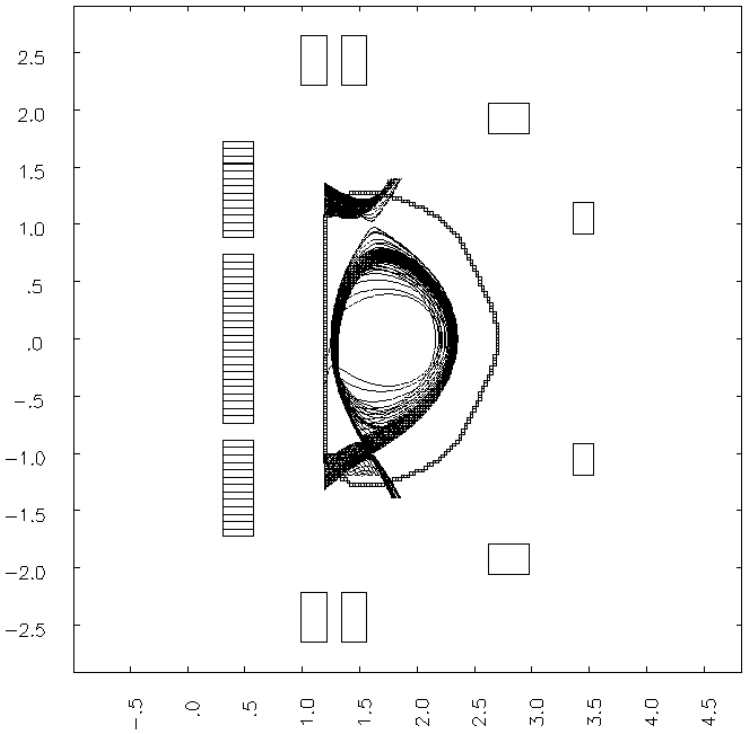

Figure 21: Snapshots of the LSN plasma/vacuum interface at various times during the evolution from 1sec to 5sec.

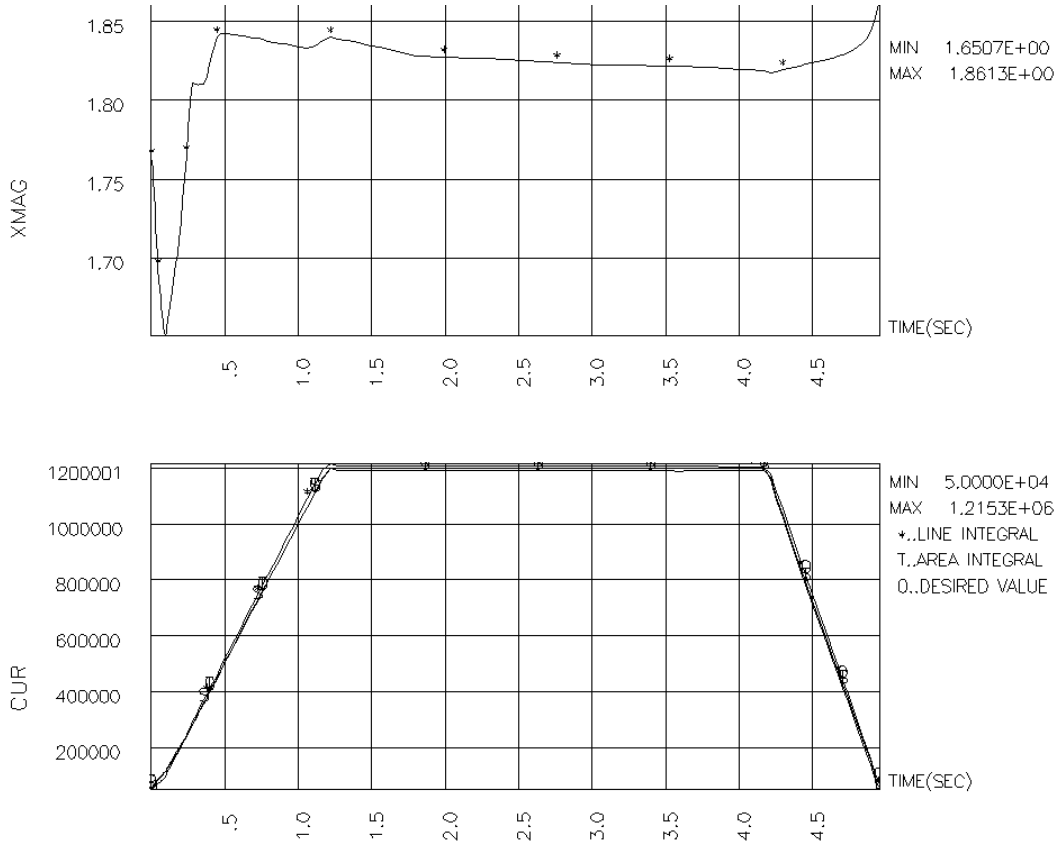

Figure 22: Evolution of plasma current CUR and plasma magnetic axis horizontal displacement XMAG in ohmic heating LSN discharge.

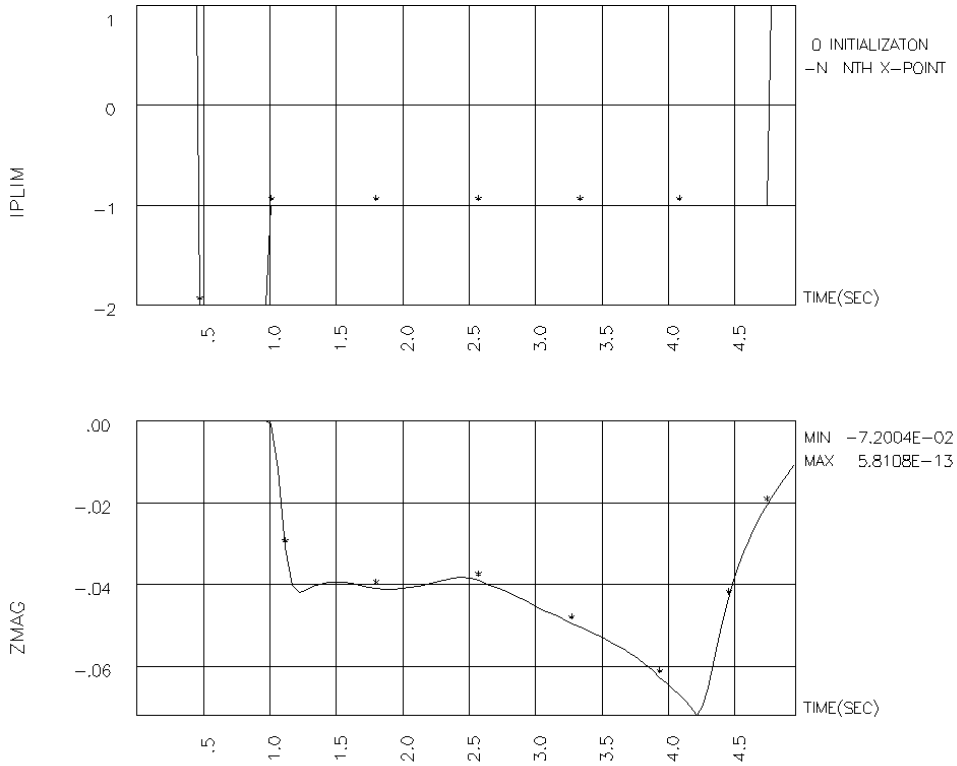

Figure 23: (Top) LSN discharge has limiter configuration (IPLIM=1.0) in the first 0.5 sec, changes to two X-point (IPLIM=-2) to 1sec and then one single null divertor configuration retains to all discharge

(IPLIM=-1.0) . (Bottom) Evolution of plasma magnetic axis vertical displacement ZMAG in ohmic heating LSN discharge.

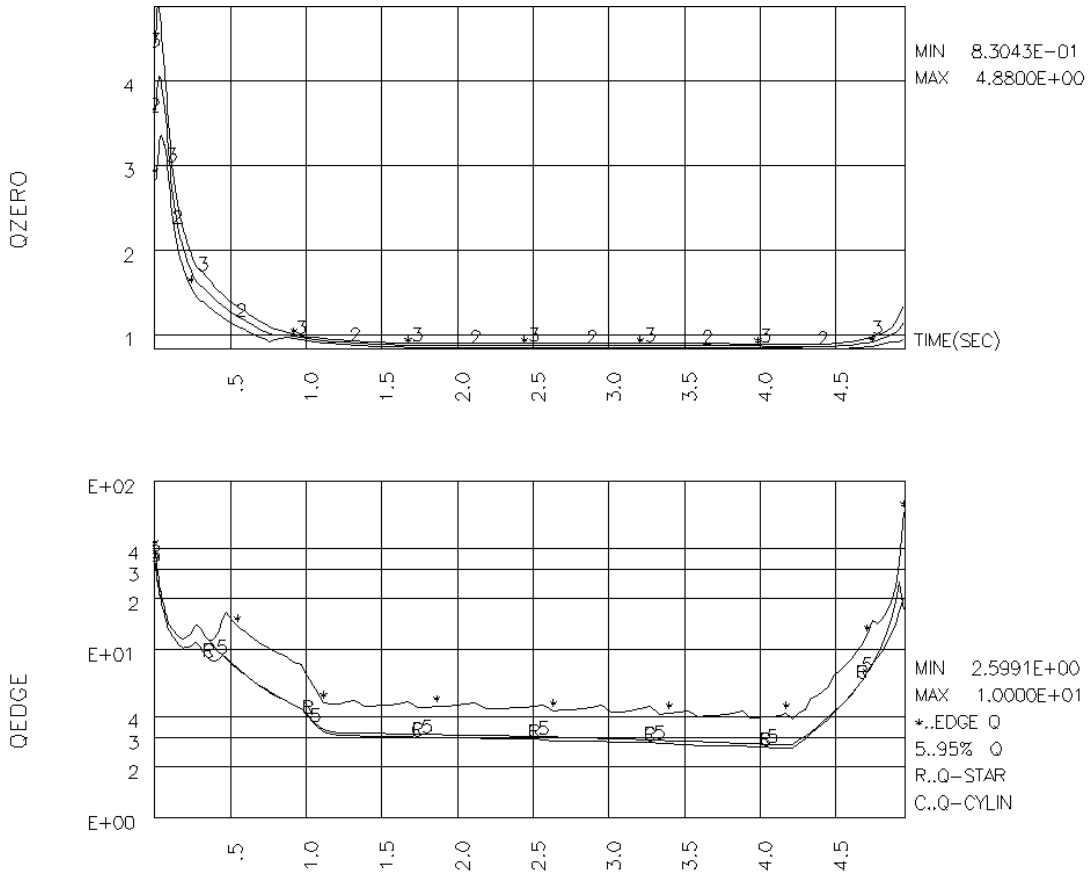

Figure 24: Evolution of plasma q factors in the plasma edge (bottom) and plasma central (top).

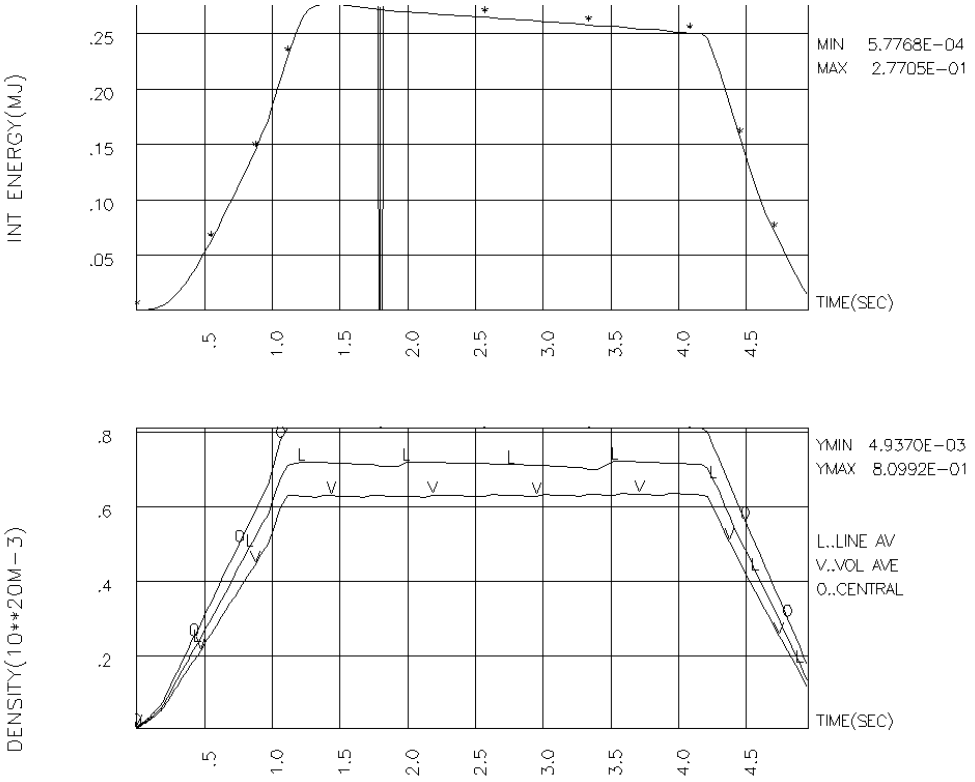

Figure 25: Evolution of plasma internal energy (top) and plasma electron density (bottom) in ohmic heating LSN discharge.

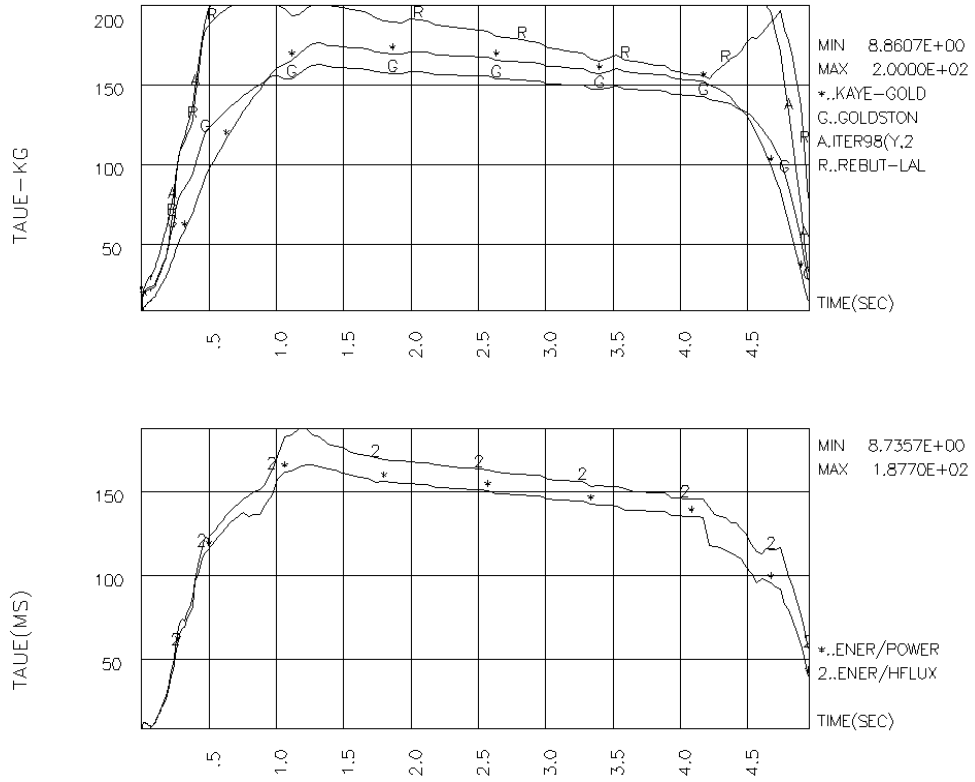

Figure . 26 Evolution of plasma energy confinement time calculated in different scaling laws.

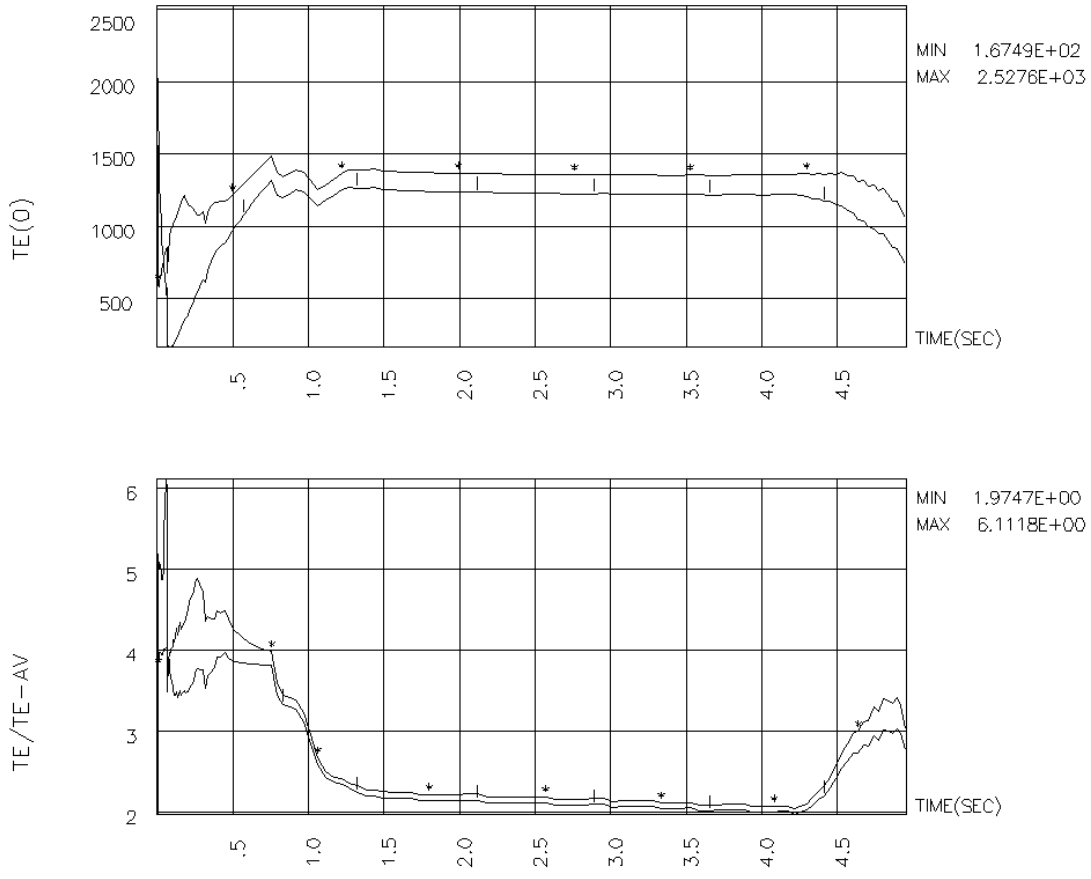

Figure. 27: Evolution of central electron and ion temperature Te, i(0) and peak to average temperatures Te,i(0)/<Te,i> for an ohmical heating LSN discharge simulation.

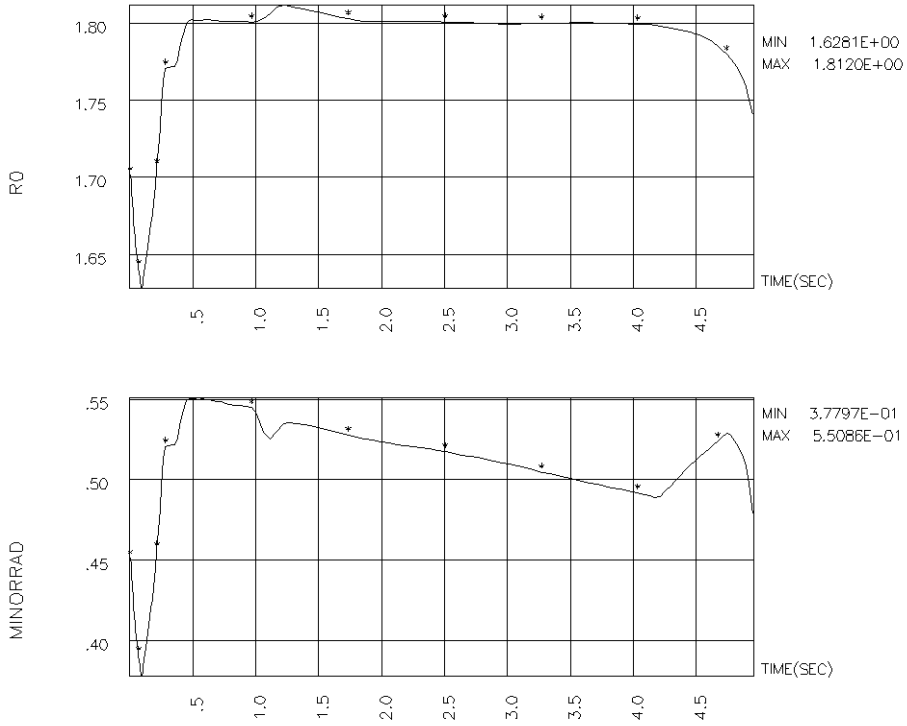

Figure 28: Evolution of major radius R0 and minor radius for the ohmic heating LSN discharge.

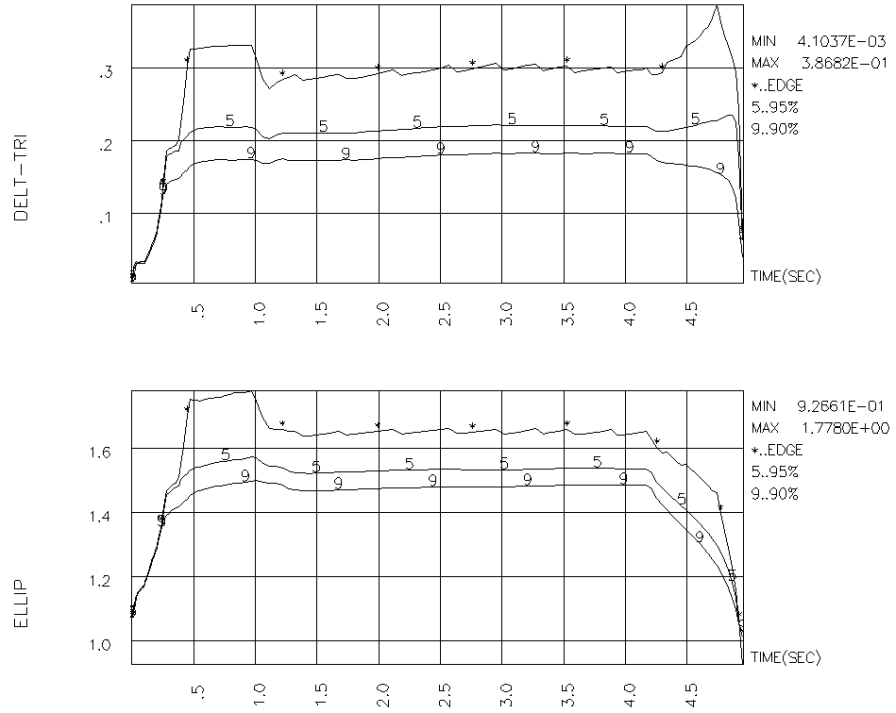

Figure 29: Evolution of triangularity (top) and elongation (bottom) for LSN ohmic discharge.

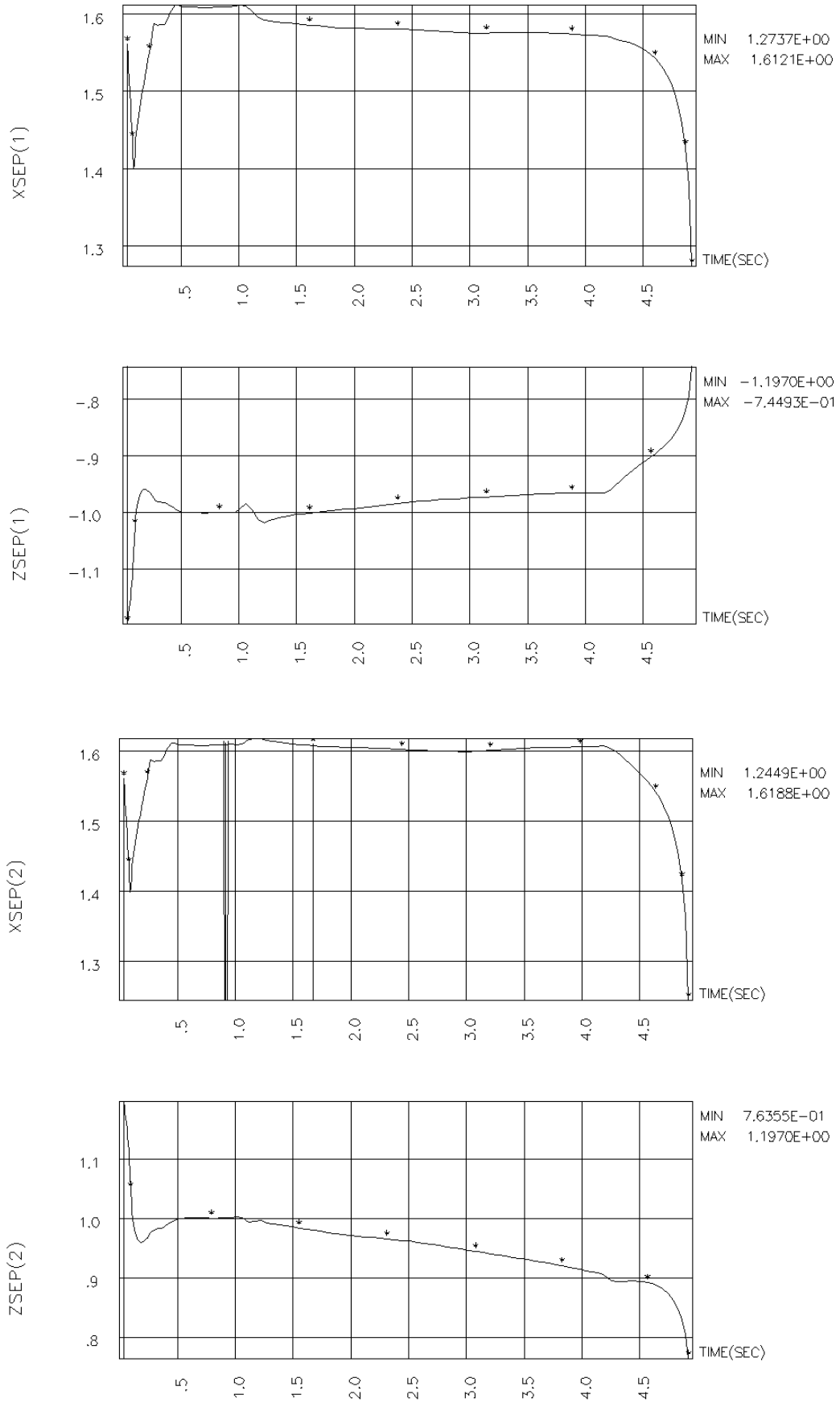

Figure. 30: Evolution of one active X-Point (top two Figures) and one inactive X-point in LSN ohmic

discharge.

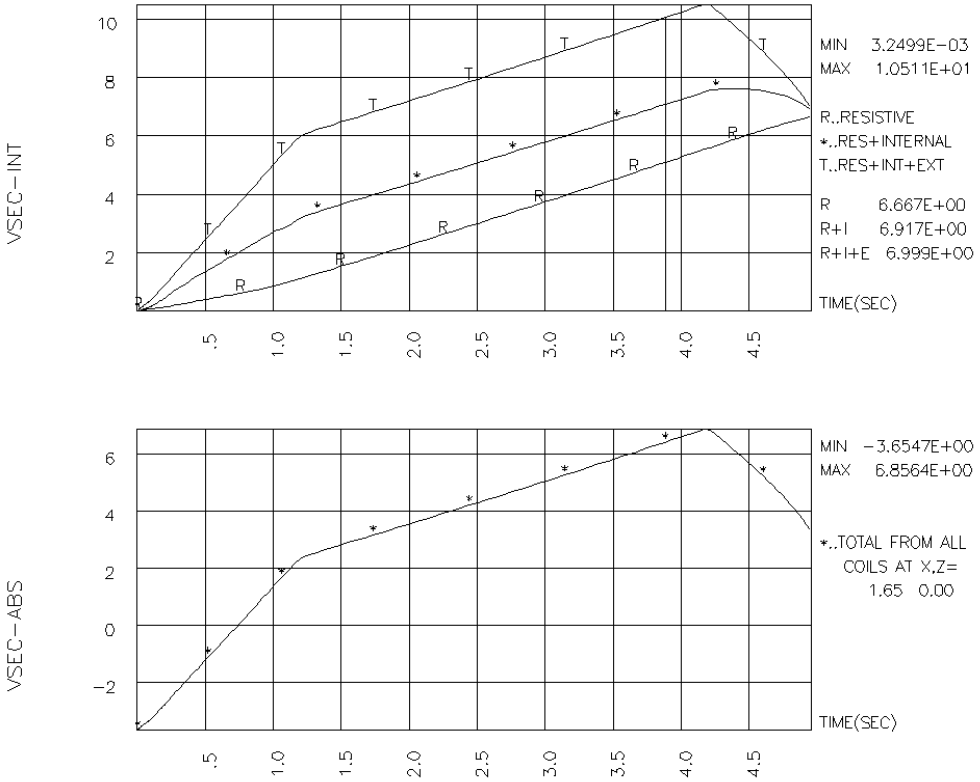

Figure 31: Evolution of Volt-seconds (top) and its absolute value.

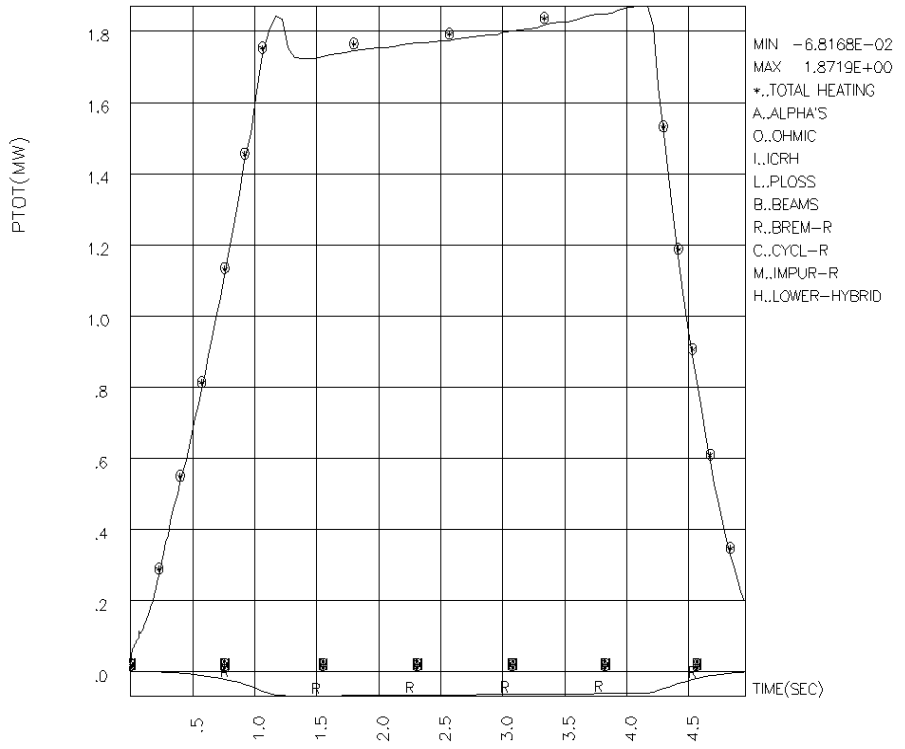

Figure 32: Plasma power balance vs. time for an ohmical LSN discharge.

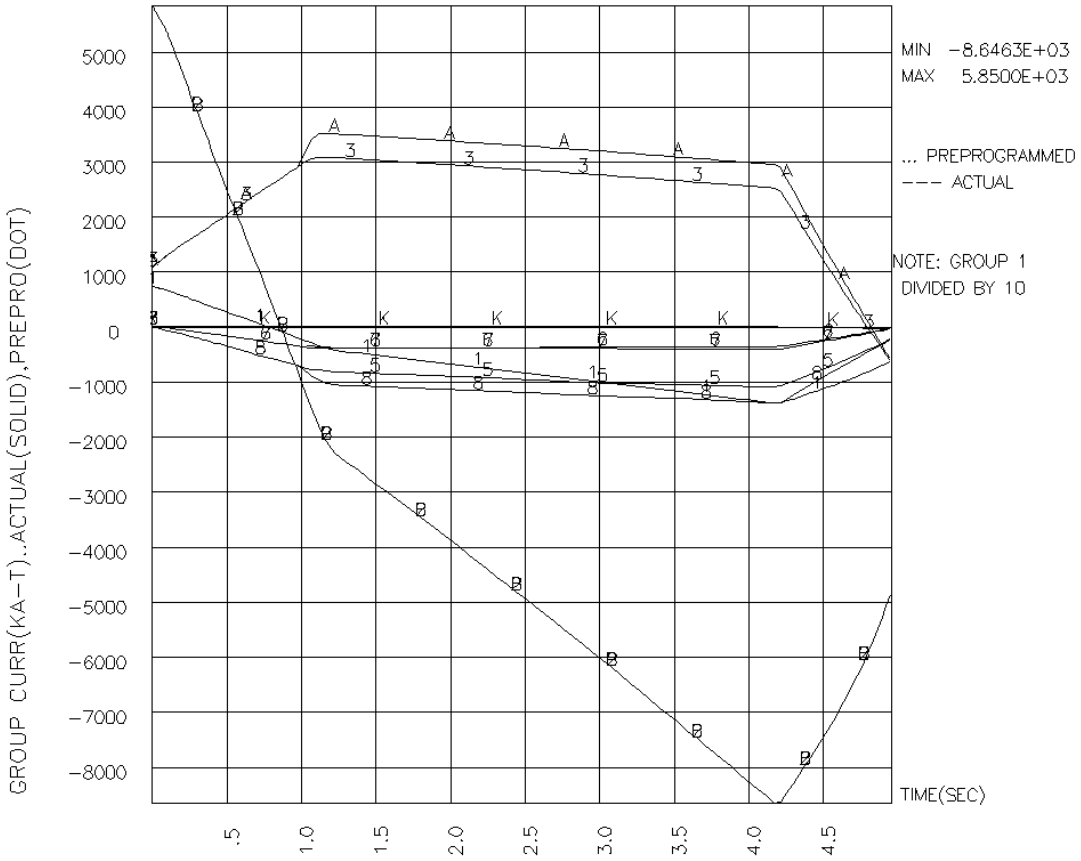

Figure 33: The histories of PF coil group currents for the ohmic heating LSN discharge.

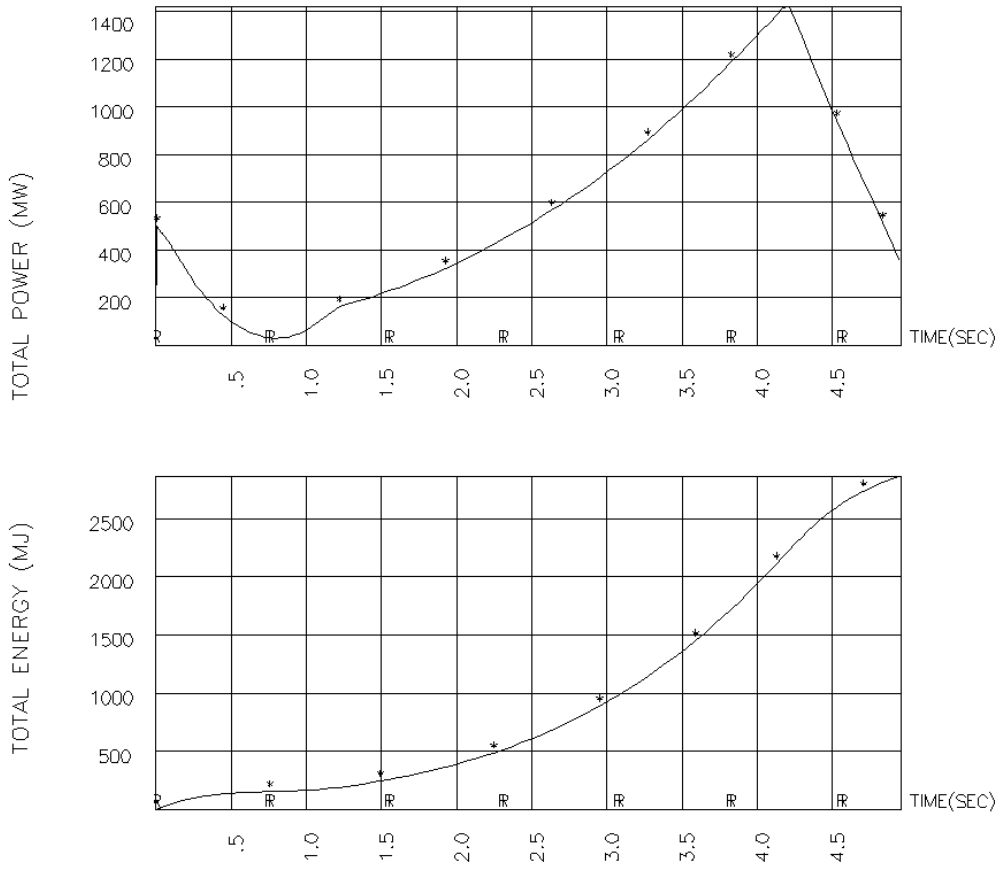

Figure 34: Evolution of total energy and total power in poloidal field coil system.

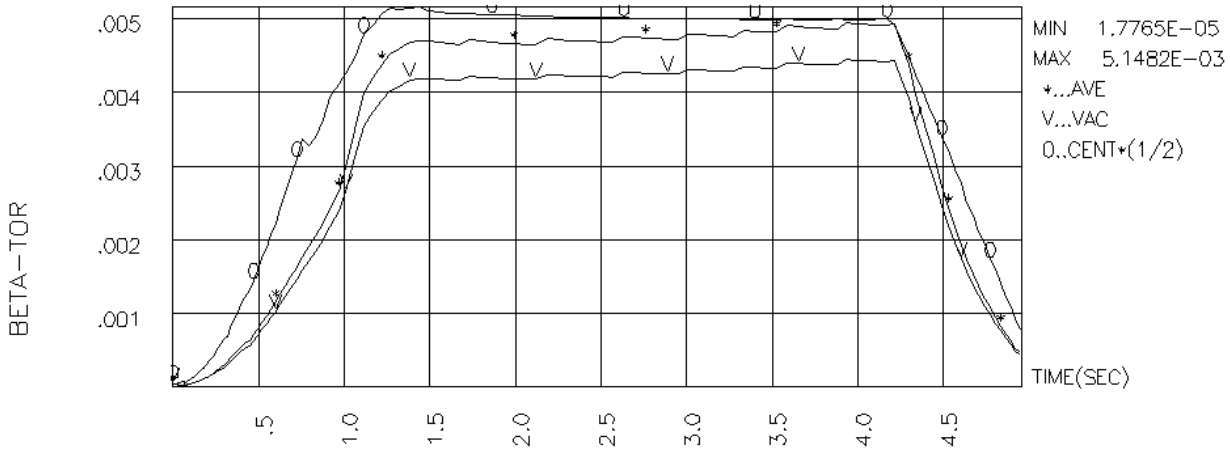

Figure.35: Evolution of one-half central beta (0), beta based on vacuum field (v), and beta based on actual toroidal field (*).

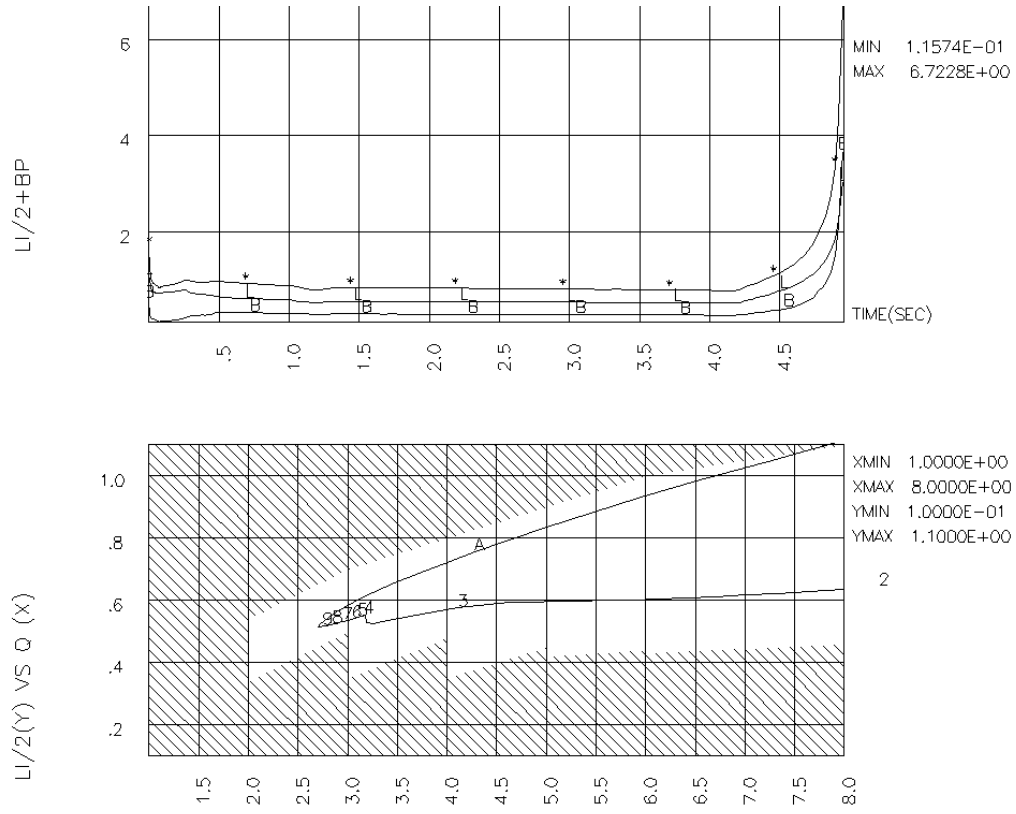

Figure 36. Top: Evolution of internal inductance $l_i/2$, poloidal beta β_p , and the sum $l_i/2+\beta_p$. Bottom: the evolution of plasma in space of internal inductance $l_i/2$ versus edge safety factor q_{95}. Unshaded region is stable according to model calculation.

IV: 3 HL-2M LSN Discharge with Auxiliary heating

Two possible DN, LSN ohmic discharges are described in the last section. The features we wish to improve upon are that the Volt-sec mainly provided by CS1, CS2 coil groups are such that

they can keep discharge no more than 3 sec. Also, in the ohmic discharges, the highest volume averaged beta is lower than 0.5%.

The HL-2M project has 10MW (4MW NB+3MW LHCD+3MW ECRH) auxiliary heating power in the first phase and 20MW auxiliary heating power is expected in the second phase. This high auxiliary heating power will not only decrease the resistive Volt-sec consumption but also will increase the plasma beta. Similarly, high power can trigger the H-Mode transition. The high beta plasma also brings other problems such as plasma stability and control. Here, we present the main results in LSN configuration with auxiliary heating power in Figures 37 through 40.

Table 6: Plasma parameter for LSN discharges with10MW auxiliary heating power (4MW NB+3MW LHCD+3MW ECRH)

	BOFT	Flattop	EOB
Time(sec)	1.0	2.5	4.25
Plasma current(MA)	1.02	1.21	1.1
Major radius(m)	1.80	1.81	1.80
Minor radius(m)	0.54	0.484	0.475
Elongation (95%)	1.59	1.724	1.642
Triangularity (95%)	0.22	0.252	0.24
Flux linkage(V-s)	5.56	7.75	8.82
Field on axis(T)	2.5	2.5	2.5
Beta β (based on actual toroidal field)	0.0025	0.00756	0.0041
Poloidal beta β_p	0.287	0.489	0.282
Internal inductance $l_i/2$	0.56	0.376	0.452
Auxiliary heating power (MW)	0.0	10.0	0.0

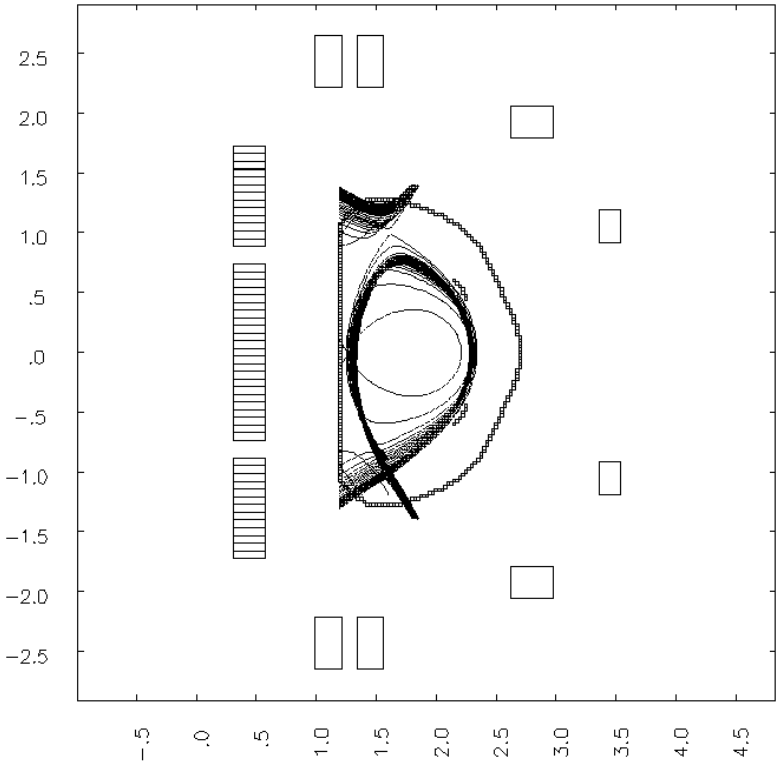

Figure 37: Snapshots of the LSN plasma /vacuum interface with 10MW auxiliary heating at various times during the evolution from 1sec to 5sec.

The basic discharge parameters still keep the same settings as that in the last two sections. To assist heating of the plasma, the following 3 kind of auxiliary heating systems are used. First, 4MW NB is turned on from the beginning of the flattop (1sec). Second, 3MW LHCD is added in the middle of flattop (1.8sec). Third, 3MW ECRH is input at flattop time 2.4 second. All of the heating systems are shut off after 3 seconds. An H-mode transition is supposed at the beginning of NB. Fig.38 shows a plot of plasma power balance as a function of time. A summary of the parameter evolution in BOFT, Flattop, EOB are listed in table 6.

Increasing the plasma beta requires an enhanced vertical feedback system and reasonable shape conditions. The gains found to yield the best response for the vertical feedback are Gp=1×10^{8} A/Wb, and Gd=1×10^{5} A-s/Wb. Strong feedback can keep the plasma magnetic axis vertical displacement stable at about 0.03~0.04m and the radial displacement stable at 1.83m with the forming of LSN from 1 second (Fig 39).

Plasma central beta quickly increased to over 1.6 % when all auxiliary heating power is added (Fig.40). At the same time, Table 6 shows $l_i/2$ decreases with the increase of β_p. Lower $l_i/2$ means the plasma has broader current profile. Very broad and very peaked profiles both alter the PF shaping field current distribution. The power requirement to the PFC system is seen to have a

directly relation with $l_i/2$. Fig 49 shows the total power provided by PF coils is decreased to half value compared with that without auxiliary heating power. The total $l_i/2+\beta_p$ has a little change during auxiliary heating. This causes q_{edge} to approach 3.0 as opposed to 3.5~4 without the auxiliary heating (Fig.48). Fig 41 also shows it to be close to the edge of the unstable region. So this operation is riskier than that without auxiliary heating power.

The electron temperature reaches 2.5keV. (Fig. 43). Plasma energy confinement time (Fig 42) decreased and plasma minor radius shrinks to about 0.48m (Fig.44). The current constitution with different heating system is demonstrated in Fig46. No big difference is found in plasma elongation and triangularity compared with that without auxiliary heating. The volt-seconds consumption is reduced (Fig 45). Fig46 shows we now have enough V-s to reach a 5seconds discharge.

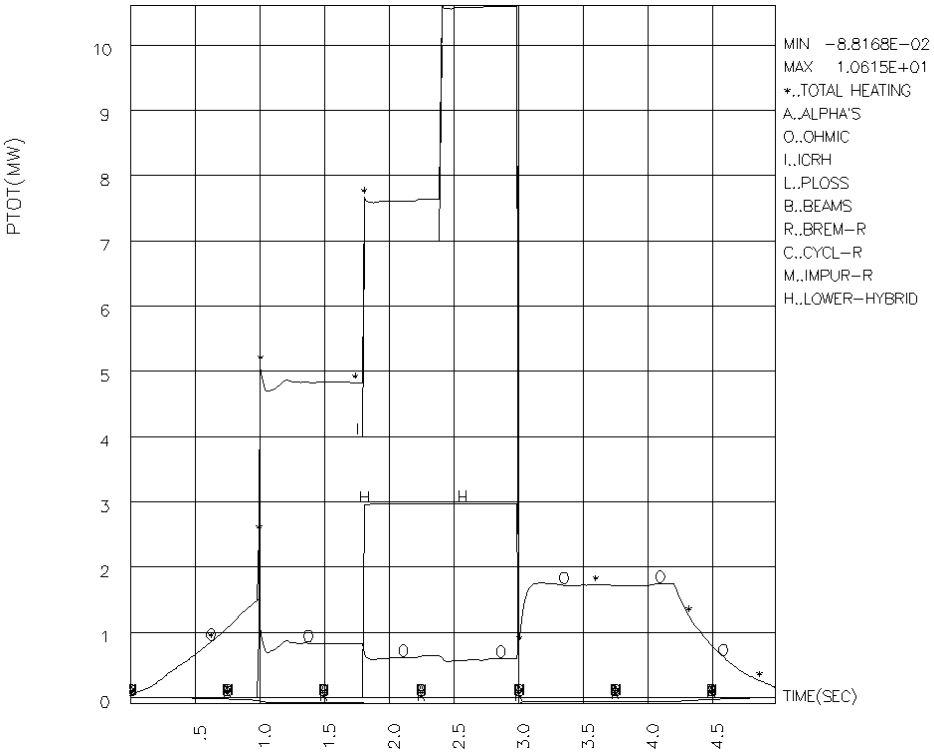

Figure 38: Evolution of Auxiliary heating power. NB: 4MW, 1~3sec, LHCD: 3MW, 1.8~3sec, ECRH: 3MW, 2.4~3sec.

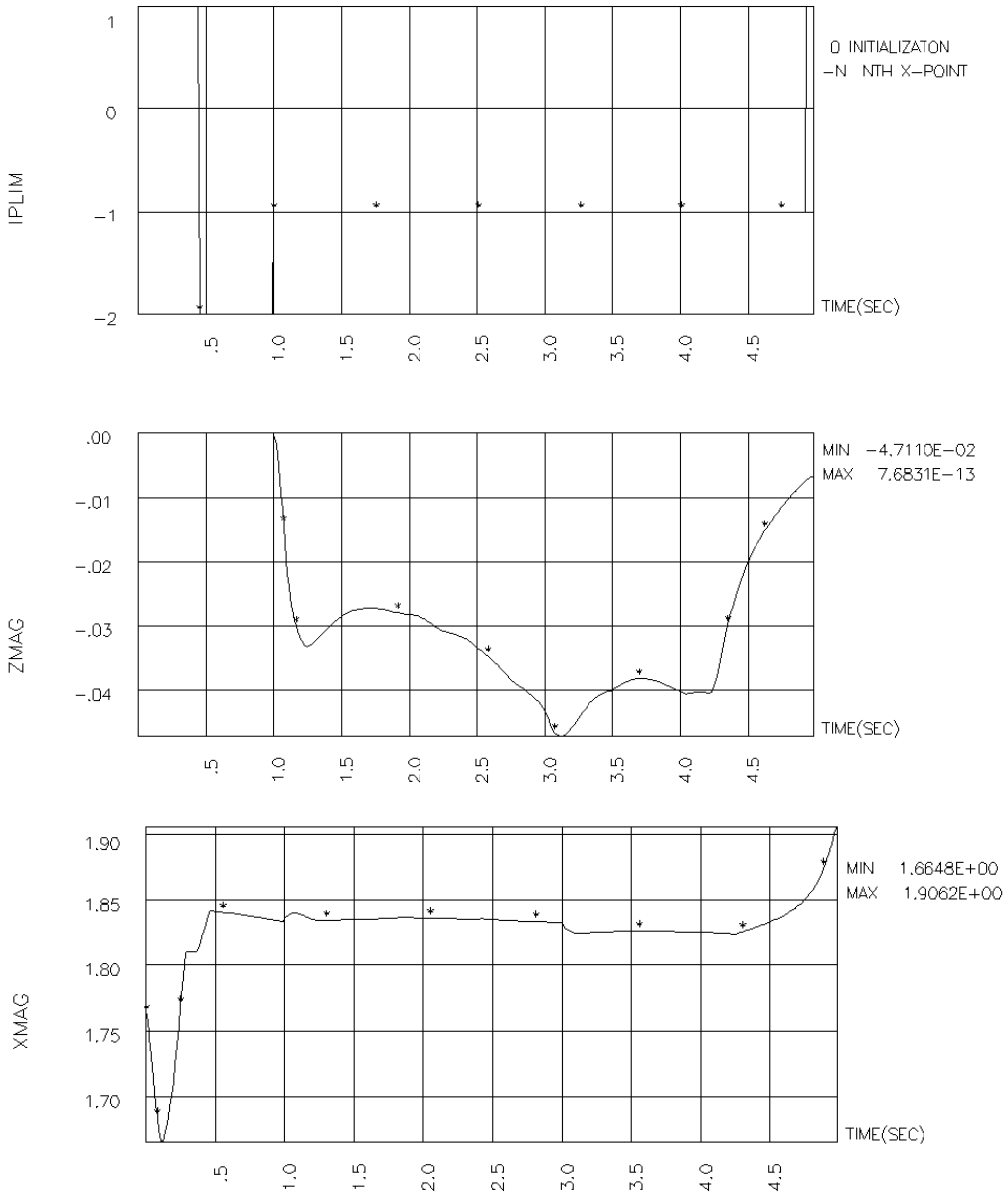

Fig.39 (Top) LSN discharge has one active X-point (IPLIM=-1) from 1second. Evolution of plasma magnetic axis vertical displacement ZMAG(middle) and horizontal displacement XMAG(bottom) in 10MW heating LSN discharge.

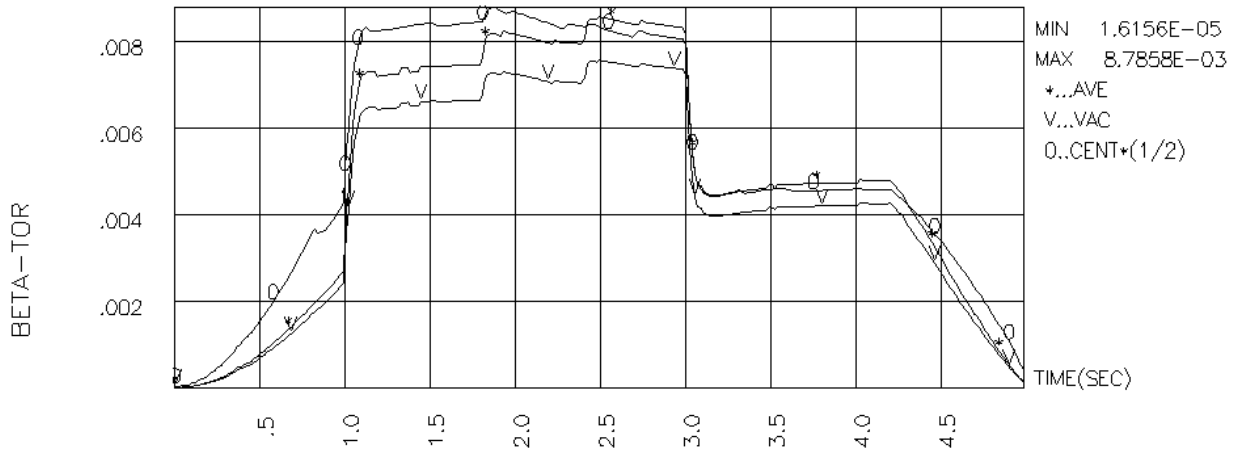

Figure 40: Evolution of one-half central beta (0), beta based on vacuum field (v), and beta based on actual toroidal field (*)

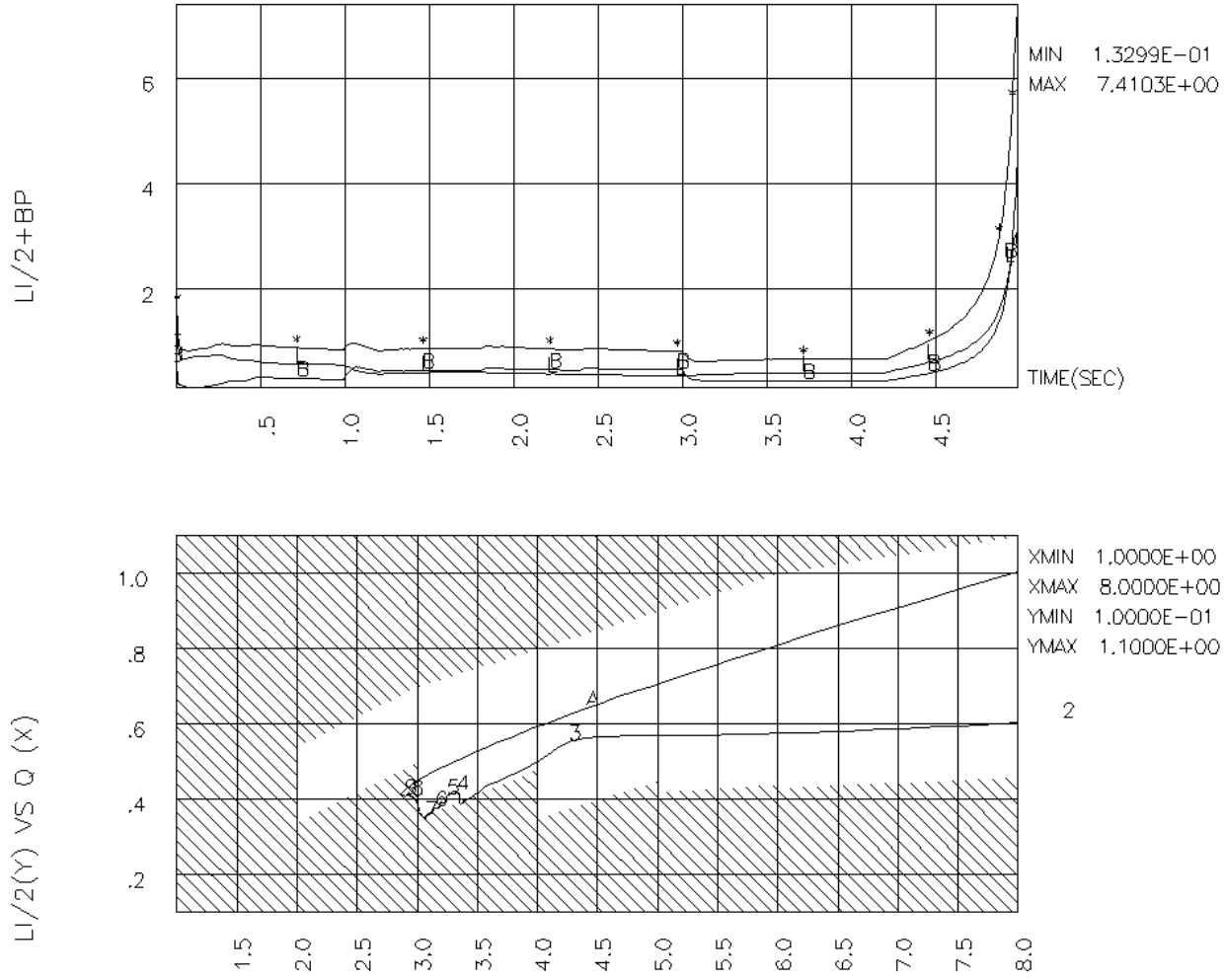

Figure 41: Top: Evolution of internal inductance $l_i/2$, poloidal beta β_p , and the sum $l_i/2+\beta_p$. Bottom: the evolution of plasma in space of internal inductance $l_i/2$ versus edge safety factor q_{95}.unshaded region is stable according to model calculation. More detail stability analysis of the equilibrium with Q95 in the range from 3.0 to 4.0 shows these equilibrium approaching the edge of unstable region.

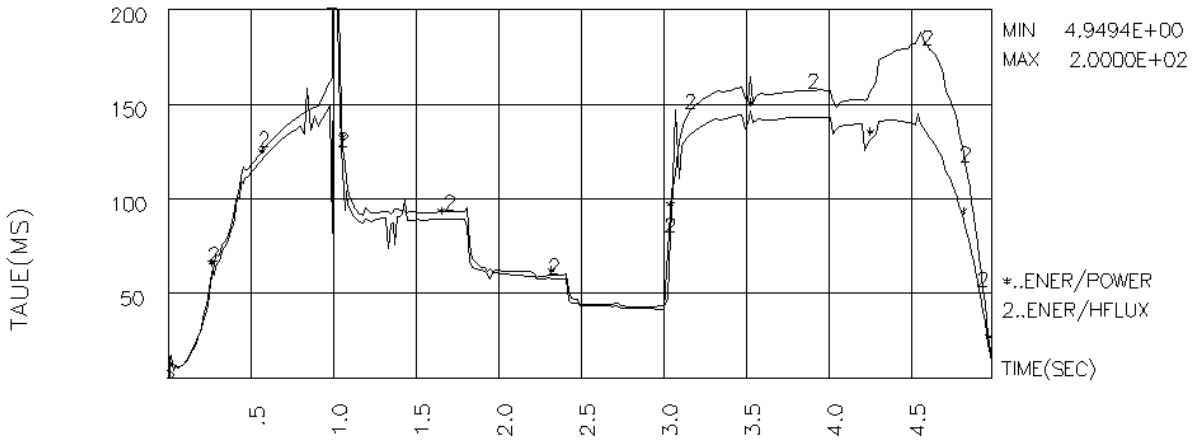

Figure 42: Evolution of plasma energy confinement time in 10MW heating LSN discharge.

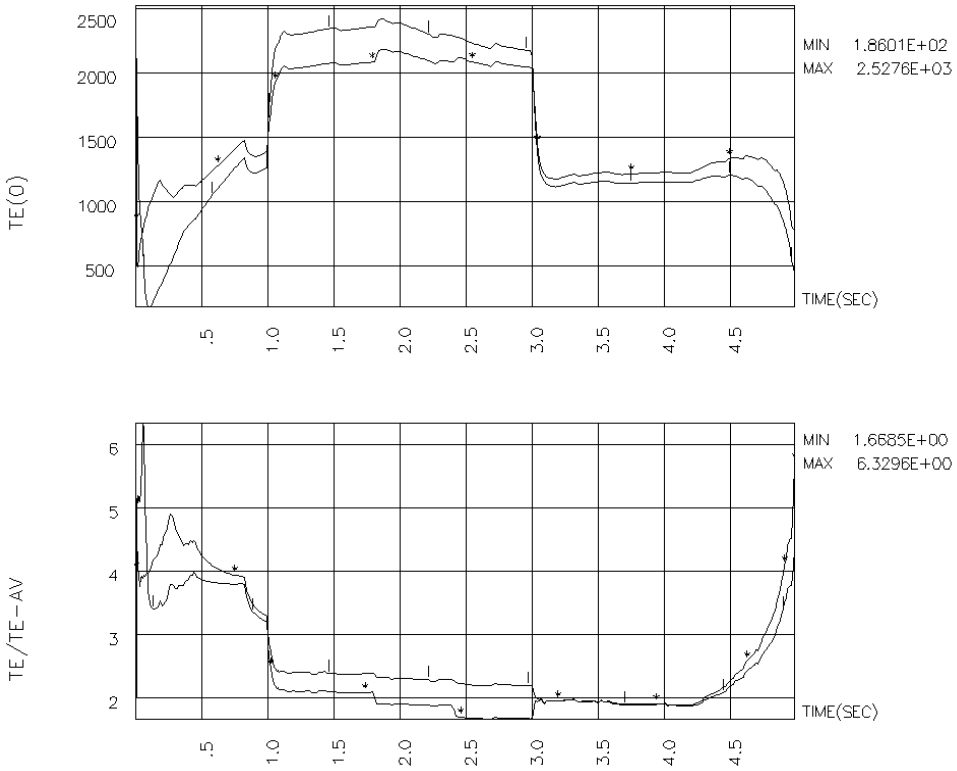

Figure 43: Evolution of central electron and ion temperature Te, i (0) and peak to average temperatures Te, i (0)/<Te, i> for LSN discharge with 10MW
auxiliary heating power input.

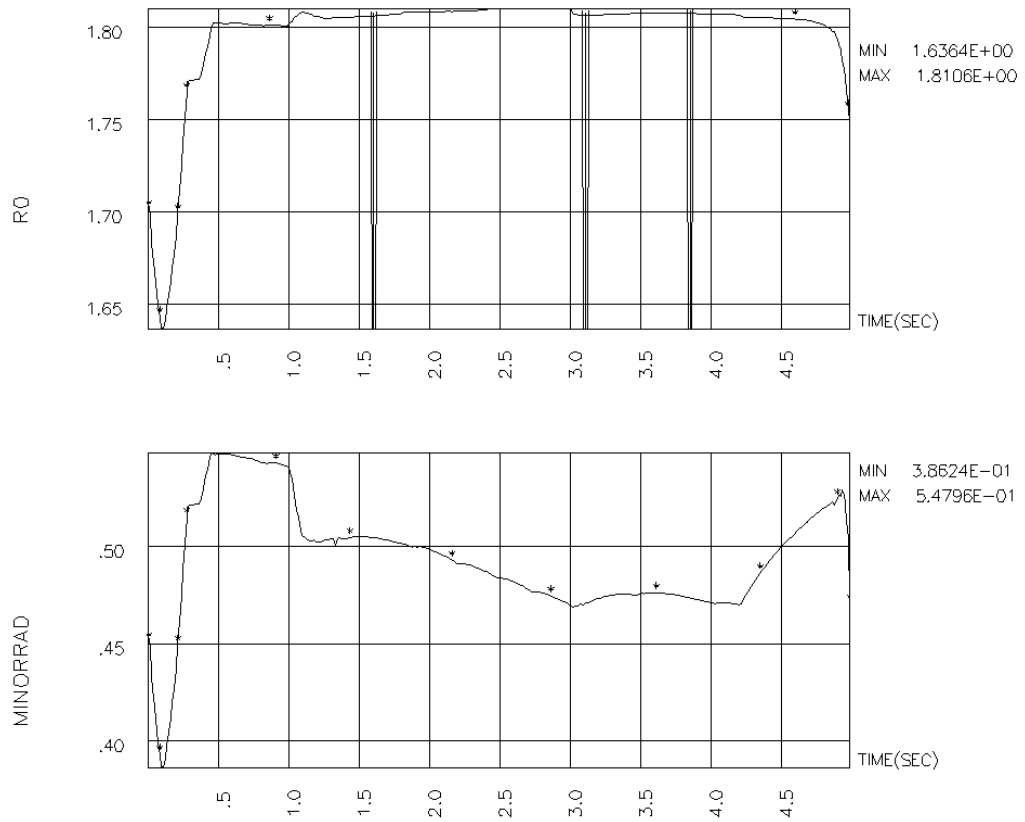

Figure. 44: Evolution of major radius R0 and minor radius for the 10MW heating LSN discharge.

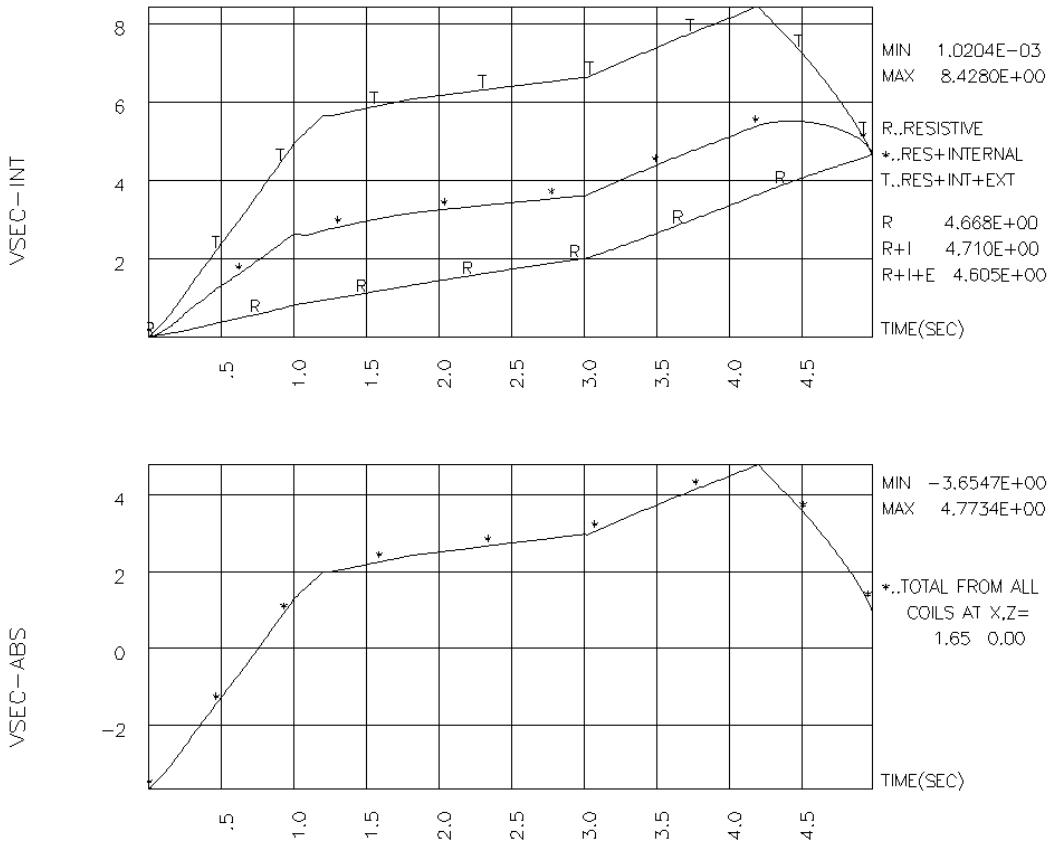

Figure. 45: Evolution of Volt-seconds (top) and its absolute value.

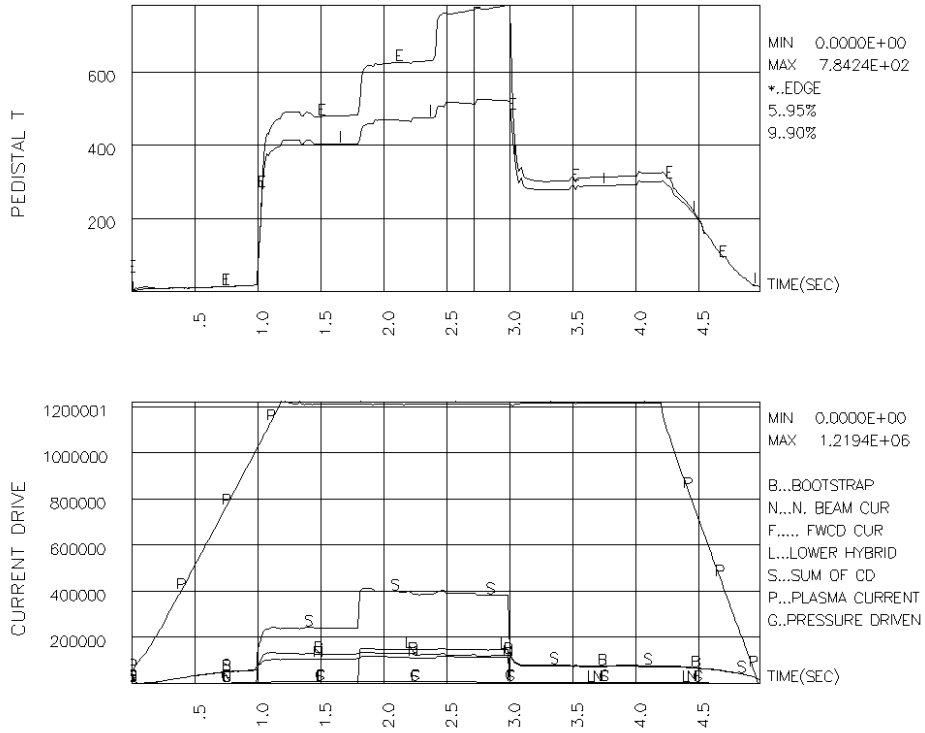

Figure. 46: Evolution of H-MODE pedestal Te(top) and plasma current constitution for 10MW heating LSN discharge.

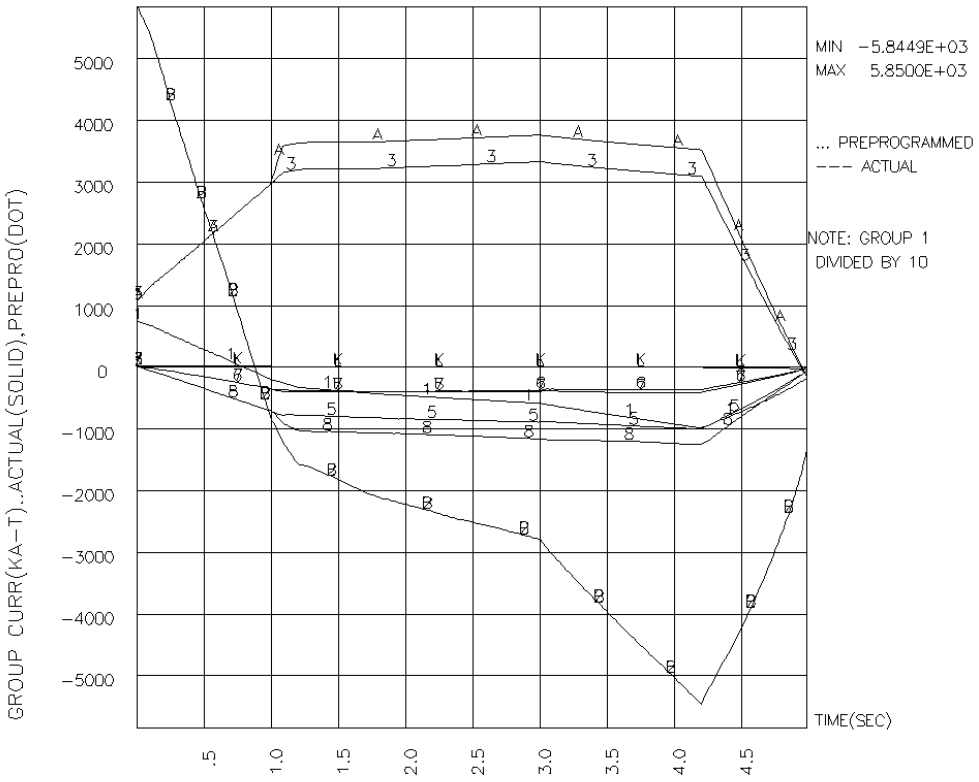

Figure 47: The histories of PF coil group currents for the LSN discharge with 10MW auxiliary heating power.

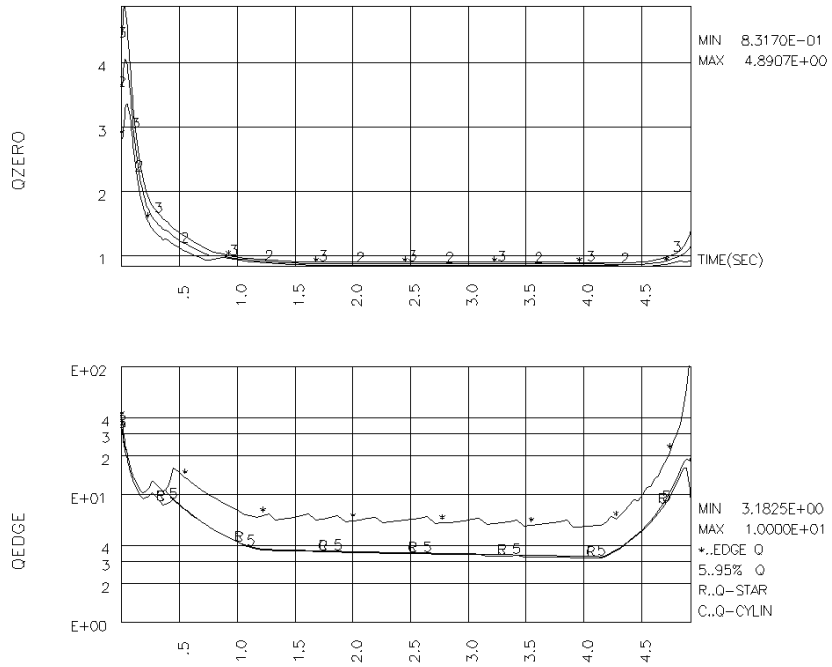

Figure 48: Evolution of plasma q factors in the plasma edge (bottom) and plasma central (top) with 10MW auxiliary heating power.

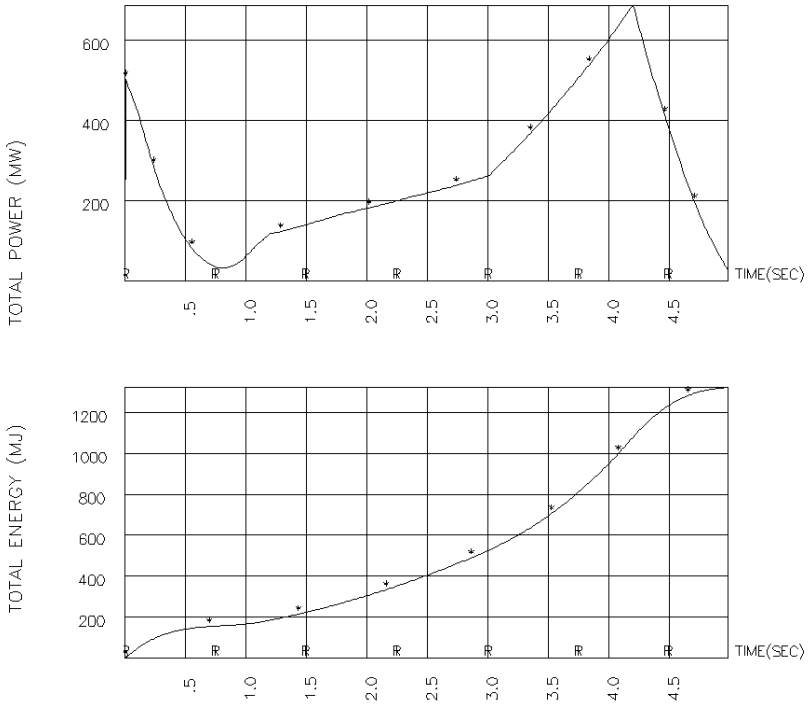

Figure 49: Evolution of total power and total energy in PFC system for 10MW heating LSN discharge.

IV.4 Vertical stability and passive plate

Vertical stability of HL-2M plasma is assessed by determining the growth time (reciprocal of growth rate) for plasma configurations inside the toroidal continuous vacuum vessel structure. The vacuum vessel is the most critical structure since it lies the closest to the plasma and is toroidally

continuous. The primary tool we used to analysis ohmic heating LSN discharge is TSC. The main procedure is the following. First, we let TSC run to flattop to get stable plasma at a fixed FFAC factor, then switch off the vertical feedback system and restart the calculation. The history of fluxes and flux different at observation pair are recorded. The vertical growth time can be deduced from the time plot of the flux difference at an observation pair.

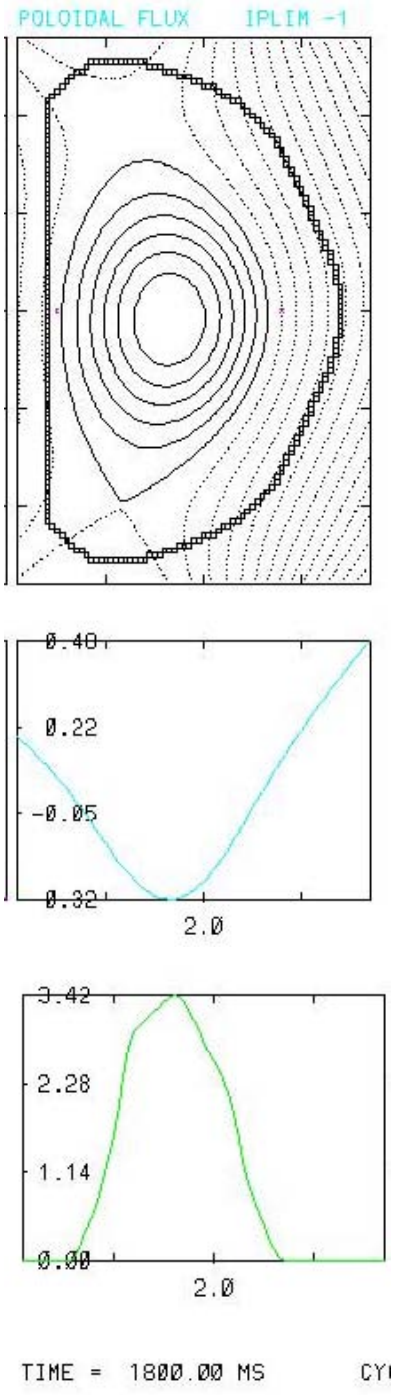

Figure 49. Plasma flux surface contours inside the TSC representation of the vacuum vessel during flattop.

Shown in Fig. 49 are the plasma flux surface contours inside the TSC representation of the vacuum vessel during the flattop. Also shown are the poloidal flux (middle) and current density

(bottom) across the midplane. At this time, $l_i/2 = 0.55$, $\beta_p = 0.284$, beta based on actual toroidal field $\beta = 0.042\%$, $k_{95} = 1.52$, $\delta_{95} = 0.21$. We show the growth time of the vertical instability in the absence of any active control coils or additional passive plates in Fig.50 as a function of the mass enhancement factor FFAC. Here, FFAC can be interpreted as the factor by which Alfven waves are artificially slowed down in the TSC code. In the TSC code, the ion mass is increased by $FFAC^2$ so that a larger stable time step can be used when computing resistive phenomena. The physical growth time should correspond to the limit as FFAC → 1. We see from Fig. 50 that as FFAC decreases, the vertical mode growth time also decreases, but appears to be converging to the physical value of ~ 2.5ms as FFAC → 1. Also, we observe that when we double the resistance of vacuum vessel, the growth time at the same FFAC decreases approximately as $1/\eta_{vv}$, where η_{vv} is the resistivity of vacuum vessel.

Thus, since the converged growth time is much greater than an Alfven wave transit time and scales with the inverse vessel resistivity, we conclude that the HL-2M design is stable on the ideal MHD timescale. However, the physical growth time is very short and is likely too fast to be controlled by an active control system with reasonable power. We would therefore recommend considering the addition of additional passive plates in order to increase the passive growth time and hence ease the control requirements for the active control system.

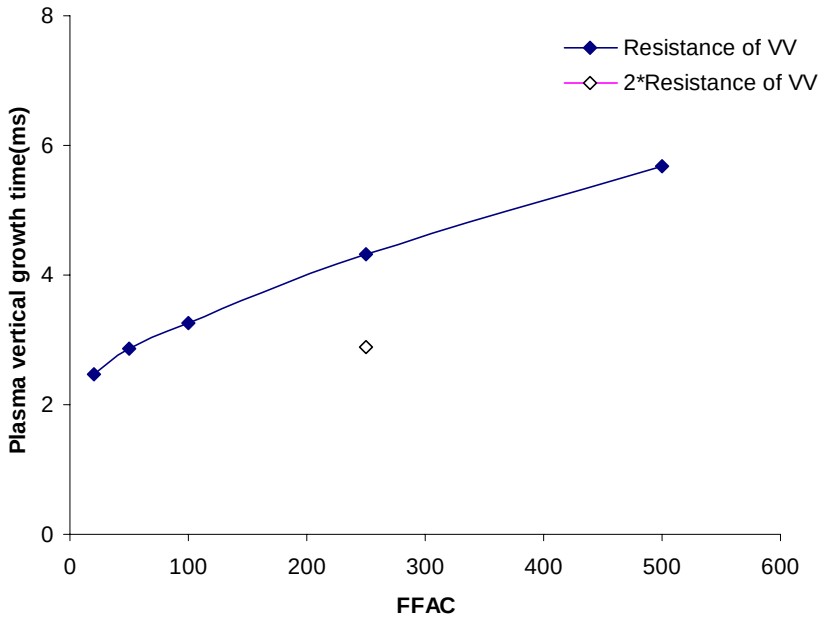

Figure. 50 Variation of the plasma vertical growth time with vacuum vessel vs. FFAC factor.

The detailed design of the HL-2M vacuum vessel is not yet fixed, but in these studies we used an 8mm thickness SS plate to estimate the resistivity of the vacuum vessel. TSC can also

model the additional passive plates that may be added to further stabilize the vertical mode. The passive plates will likely consist of two plates installed between the plasma edge and vacuum vessel, symmetric with respect to the midplane. In order to decrease to the coupling to the other PFC coils, the passive plates should be constructed (and modeled) to have a zero net current constraint. This corresponds to one or more cuts at a fixed toroidal angle. The proposed plate material is copper with thickness 0.05m. The plates being considered pass through the positions (2.17, ± 0.57), (2.2, ± 0.52) and (2.23, ± 0.47). A future study will evaluate the effectiveness of these plates in controlling the vertical instability.

V. Summary of equilibrium capability

The last section has presented the main calculation results and the actual coil and plasma currents needed to satisfy the performance requirements. The reference operating modes are the DN divertor and the SN divertor with ohmic or auxiliary heating power. The results show that the discharge can be smoothly transformed from a limiter to a DN/LSN configuration and then ramped down again without a disruption.

It has long been recognized that MHD stability consideration are an important part of device design. The plasma parameters significant to MHD stability are the plasma geometry, safety factor at the plasma edge, toroidal beta and the plasma pressure and current profiles. Of these factors, the total plasma current (or edge safety factor) is one of the most critical. When the plasma current is such that q_{edge} <2, the discharge is almost certain to disrupt. These disruptions are primarily due to current-driven external kink modes and are not related to beta effects. Operations at 2< q_{edge} <3 requires great care to avoid frequent disruption. However, when q_{edge} >3, disruptions can generally be avoided. For HL-2M, The nominal total plasma current is 1.2MA which corresponds to an edge safety factor q_{edge} between 3 and 4. MHD stability analysis shows this regime to be stable.

If just ohmic heating is considered, based on the basic current ratios provided by EFIT calculation, HL-2M can have good DN or LSN divertor discharge from t=0.5sec and it can be retained at least 3.0 seconds according to the Volt-sec consumption. Without auxiliary heating, the highest plasma central beta is 1.0 %, the lowest q_{edge} is about 3.5, and discharges should be stable.

The LSN divertor configuration is the primary HL-2M operation mode. A reference discharge simulation with 10MW auxiliary heating power is shown in section IV.3. High auxiliary heating power can save Volt-seconds to allow a 5 seconds discharge. The higher beta (β), lower internal

inductance ($l_i/2$) and lower edge safety factor (q_{edge}=3.0) make the discharge operation approach the edge of instability.

The simple passive plate system using only the vacuum vessel is discussed in section IV.4. TSC predicts that the HL-2M design without additional passive plates is ideal MHD stable to the vertical instability, but with a very short growth time. Additional more detailed studies should be performed in order to optimize the shape and location of these plates and to evaluate and optimize the properties of the active control system.

VI. Acknowledgements

This work was supported by U.S. DoE contract DE-AC02-76CH03073. One of us (YP) would like to acknowledge the American-China cooperation project for the opportunity to visit Princeton Plasma Physics Laboratory (PPPL) for 3 months.

References

[1] Jardin,S.C., DeLucia J, and Pomphrey, N, J.Comput.Phys.66 (1986)481.

[2] S.C.Jardin, M.G.Bell,N.Pomphrey, TSC simulation of ohmic discharge in TFTR, Nuc.Fusion, Vol.33, No.3,(1993) ,371

[3] Willam Daughton, S.C.Jardin, C.Kessel, Neil Pomphrey, TSC users manual,1997

[4] S.C. Jardin, J.Delucia. , M.Okabayash , Nuclear Fusion 27(1987) 569

[5] F.B.Marcus, F.Hoffmann., S.C. Jardin, P.Noll, G.Tonetti, Nuclear Fusion 30(1990) 1511

[6] Hoffmann. F., S.C. Jardin , Nuclear Fusion 30(1990) 2013

[7] S.C. Jardin, M.G.Bell, J,L. Johnson, S.M.Kaye, C.Kessel, etal, Fusion Technology, 21 (1992) 1123

[8] C.Kessel, S.C. Jardin, R.H.Bulmer, R.D.Pillsbury, P.W.Wang, G.H.Neilson, D.J.Strickler Fusion Technology, 30 (1996) 184

[9] S.C. Jardin, "KSTAR plasma equilibrium, stability and control", presented at KSTAR Physics Validation Review, PPPL,1997.6.23

[10] R.O.Sayer, Y.K.Peng, S.C. Jardin, A.G.Kellman, J.C.Wesley, Nuclear Fusion 33(1993) 969

[11] S.C. Jardin, C.Kessel, N.Pomphrey, Nuclear Fusion 34(1994) 1145

[12] D.J. Ward, E.J.Valeo, S.C. Jardin, Nuclear Fusion 34 (1994) 837

[13] S.C. Jardin, G.L.Schmidt, E.D.Fredrickson, K.W.Hill, J.Hyum, BJ.Merril, R.Sayer, Nuclear Fusion 40 (2000) 923

[14] S.C.Jardin, W.Park, Phys. Fluids 24 679 (1981)
[15] S.C.Jardin, J. Comput. Phys. 43, 31 (1981)
[16] S.P.Hirshman, Phys. Fluids 31 3150 (1988)
[17] D.J.Ward, S.C.Jardin, Nuclear Fusion 32 973(1992)

The Princeton Plasma Physics Laboratory is operated
by Princeton University under contract
with the U.S. Department of Energy.

Information Services
Princeton Plasma Physics Laboratory
P.O. Box 451
Princeton, NJ 08543

Phone: 609-243-2750
Fax: 609-243-2751
e-mail: pppl_info@pppl.gov
Internet Address: http://www.pppl.gov